NEUROSCIENCE

eNAMPT actions through nucleus accumbens NAD$^+$/SIRT1 link increased adiposity with sociability deficits programmed by peripuberty stress

Laia Morató[1]*, Simone Astori[1]†, Ioannis Zalachoras[1]†, Joao Rodrigues[1], Sriparna Ghosal[1], Wei Huang[2], Isabelle Guillot de Suduiraut[1], Jocelyn Grosse[1], Olivia Zanoletti[1], Lei Cao[2], Johan Auwerx[3], Carmen Sandi[1]*

Obesity is frequently associated with impairments in the social domain, and stress at puberty can lead to long-lasting changes in visceral fat deposition and in social behaviors. However, whether stress-induced changes in adipose tissue can affect fat-to-brain signaling, thereby orchestrating behavioral changes, remains unknown. We found that peripubertally stressed male—but not female—mice exhibit concomitant increased adiposity and sociability deficits. We show that reduced levels of the adipokine nicotinamide phosphoribosyltransferase (NAMPT) in fat and its extracellular form eNAMPT in blood contribute to lifelong reductions in sociability induced by peripubertal stress. By using a series of adipose tissue and brain region–specific loss- and gain-of-function approaches, we implicate impaired nicotinamide adenine dinucleotide (NAD$^+$)/SIRT1 pathway in the nucleus accumbens. Impairments in sociability and accumbal neuronal excitability are prevented by normalization of eNAMPT levels or treatment with nicotinamide mononucleotide (NMN), a NAD$^+$-boosting compound. We propose NAD$^+$ boosters to treat social deficits of early life stress origin.

INTRODUCTION

The period comprising late childhood and puberty (herein, peripuberty) is a critical time window of brain development (*1*) and adipose tissue maturation (*2*). Chronic stress during peripuberty is a risk factor for adult psychopathology, particularly dysfunctional social behavior (*3*, *4*). On the other hand, increased fat mass (*5*) and obesity (*6*) have been reported in adults exposed to adverse experiences during peripuberty.

Although obesity is frequently associated with impairments in the social domain in humans (*7*, *8*), it is difficult to establish whether these metabolic and behavioral alterations are independent or causally related. Nonbiological explanations such as prejudice or discrimination (*9*) have been put forward to explain social withdrawal observed in overweight individuals. However, given the transactional character of social behaviors, it is particularly challenging to discern to what extent social withdrawal is elicited by the concerned individual or by its social environment. In addition, the contribution of biological factors to this association is unclear. Animal studies can help disentangle both the specific contribution of the overweight individual to the behavioral phenotype and the potential biological factors underlying the association between obesity and impaired sociability.

In this study, we investigate the molecular mechanisms whereby the increase in adiposity induced by peripubertal stress triggers long-lasting changes in social behavior. Adipose tissue is an active organ that secretes adipokines, endocrine factors capable of coordinating responses between the adipose tissue and other organs, including the brain (*10*). Among them, eNAMPT corresponds to the enzymatically active extracellular form of nicotinamide phosphoribosyltransferase (NAMPT) (*11*). NAMPT has been involved in the pathophysiology of obesity and is a rate-limiting nicotinamide adenine dinucleotide (NAD$^+$) biosynthetic enzyme (*11*). NAD$^+$ is an essential regulator of cellular metabolism and a rate-limiting substrate for the activity of the deacetylase Sirtuin 1 (silent mating type information regulation 2 homolog; SIRT1) (*12*). Notably, eNAMPT is secreted from adipocytes to the systemic circulation in extracellular vesicles and internalized in the hypothalamus, where it promotes NAD$^+$ synthesis and SIRT1 activity (*13*, *14*). In its turn, SIRT1 regulates a wide range of neurophysiological processes including neurodevelopment, synaptic plasticity, and mitochondrial function (*15*). Likewise, peripheral administration of nicotinamide mononucleotide (NMN)—a NAD$^+$ booster compound that corresponds to the enzymatic product of NAMPT—has been shown to increase NAD$^+$ levels in the brain and rescue the behavioral alterations associated with neurodegenerative conditions (*16*). However, it remains unexplored whether early life stress can reprogram adult behavior through an impairment of the eNAMPT/NAD$^+$/SIRT1 pathway.

Here, we contribute a novel mouse model—on the basis of exposure to stress during the peripubertal period—that recapitulates concomitant increased adiposity and sociability deficits, as frequently reported in humans, and investigate the mechanistic underpinnings of this association. We show that, in male mice, peripubertal stress–induced increase in adiposity is accompanied by reduced eNAMPT levels and impaired NAD$^+$/SIRT1 pathway in the nucleus accumbens (NAc), a brain region known to encode the rewarding properties of social behavior (*17*). Further, we demonstrate that adipose tissue–specific normalization of NAMPT levels or dietary treatment with NMN in peripuberty stressed mice normalizes the alterations in sociability and neuronal excitability through an activation of the NAD$^+$/SIRT1 pathway in the NAc. Our findings highlight the adipokine eNAMPT as a molecular mediator of the reprogramming

[1]Laboratory of Behavioral Genetics, Brain Mind Institute, Ecole Polytechnique Fédérale de Lausanne (EPFL), CH-1015 Lausanne, Switzerland. [2]The Comprehensive Cancer Center, The Ohio State University, Columbus, OH 43210, USA. [3]Laboratory of Integrative Systems Physiology, Institute of Bioengineering, Ecole Polytechnique Fédérale de Lausanne (EPFL), CH-1015 Lausanne, Switzerland.
*Corresponding author. Email: carmen.sandi@epfl.ch (C.S.); laia.moratofornaguera@epfl.ch (L.M.)
†These authors contributed equally to this work.

effects of early life stress on social behavior and the nexus between increased adiposity and this behavioral phenotype.

RESULTS

Peripuberty stressed mice show reduced sociability and increased adiposity

We first aimed at identifying a mouse model that recapitulates the association between increased adiposity and social deficits, frequently observed in humans. To this end, we exposed peripubertal mice to chronic unpredictable stress (CUS) (Fig. 1A) and subsequently evaluated their metabolic and behavioral phenotypes. At adulthood, stressed male mice exhibited reduced sociability (Fig. 1, B and C, and fig. S1A), in the absence of changes in general behavior (fig. S1, B to H). During the period of stress exposure (i.e., peripubertal period), stressed mice showed reduced body weight (fig. S1I). These differences in body weight were normalized at adulthood (Fig. 1D). However, analysis of body composition in adult mice revealed an increase in absolute and percentage of fat mass (Fig. 1, E and F) and a reduction in absolute and percentage of lean mass (fig. S1, J and K) in stressed mice, although no changes in body weight. Percentage of fat mass negatively correlated with sociability at adulthood (fig. S1L). Abdominal micro–computed tomography (microCT) indicated increased volume of visceral and subcutaneous fat depots (Fig. 1, G and H), and hematoxylin and eosin staining of epididymal white adipose tissue (eWAT) showed adipocyte hypertrophy (Fig. 1, I and J) in stressed mice. These metabolic alterations were observed along with reduced food intake (fig. S1M), mild glucose intolerance (fig. S1O), normative glucose levels following insulin injection (fig. S1P), and lower respiratory exchange ratio (RER) measured by indirect calorimetry (fig. S1, Q to Y). Females exposed to the same protocol of stress at peripuberty did not show remarkable differences in behavior or body composition at adulthood (fig. S2). In summary, our model of peripubertal stress in male mice triggers a reprogramming

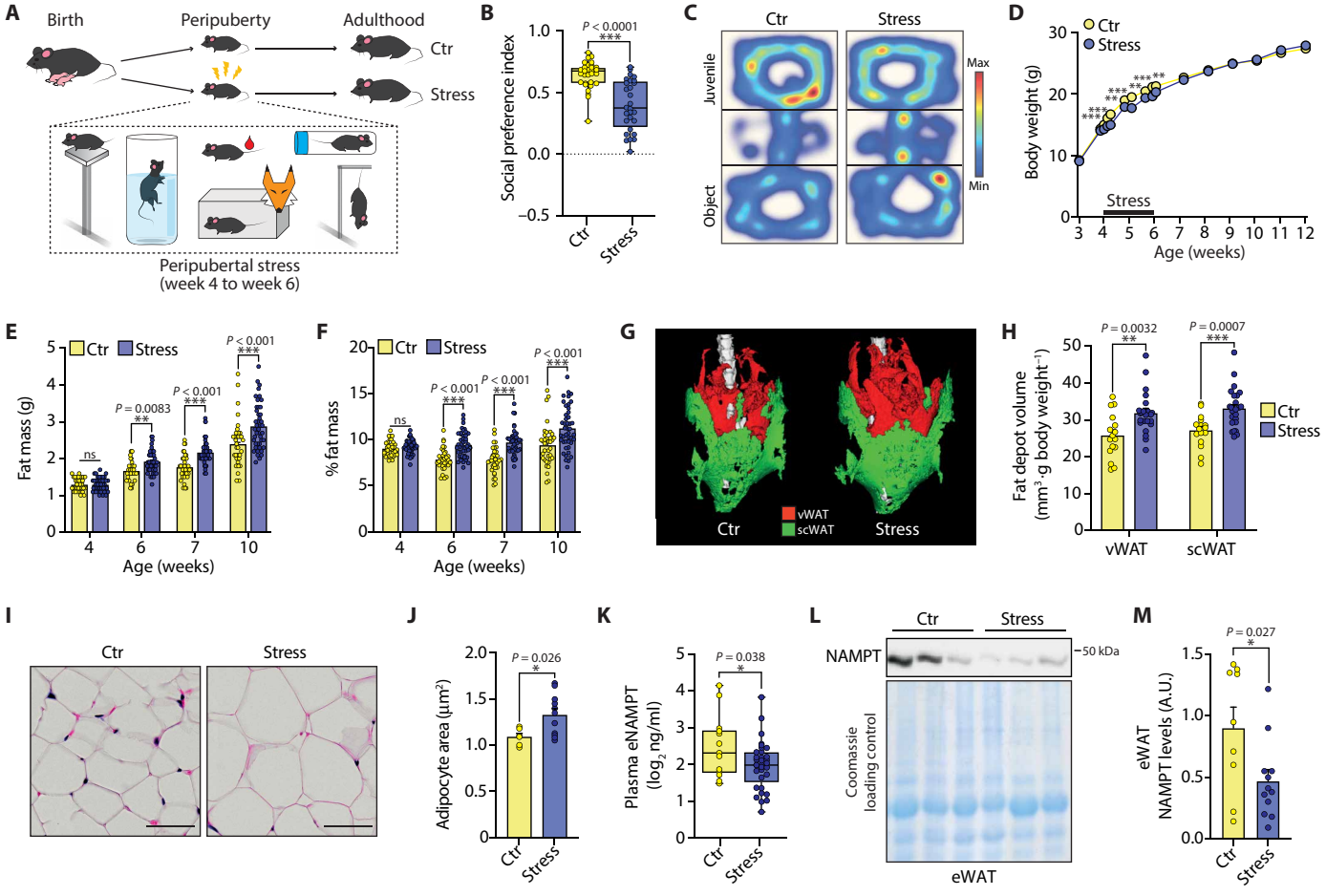

Fig. 1. Adult male mice stressed at peripuberty show changes in sociability, adiposity, blood eNAMPT, and NAD$^+$/SIRT1 pathway in the NAc. (**A**) Representative experimental timeline. (**B** and **C**) Reduced social preference index in stressed mice ($n = 31$ Ctr and 28 Stress) and representative heatmaps of mouse position during the social preference test. Adult mice stressed during peripuberty showed (**D**) no differences in body weight despite reduced body weight during the period of stress exposure. Adult stressed mice showed (**E**) higher absolute and (**F**) higher percentage of fat mass ($n = 36$ Ctr and 44 Stress), (**G** and **H**) increased visceral white adipose tissue (vWAT) and subcutaneous white adipose tissue (scWAT) volume ($n = 16$ Ctr and 24 Stress), and (**I** and **J**) adipocyte hypertrophy in eWAT ($n = 6$ Ctr and 11 Stress). Stress mice showed (**K**) reduced levels of plasma eNAMPT ($n = 13$ Ctr and 33 Stress) and (**L** and **M**) NAMPT in eWAT ($n = 9$ Ctr and 12 Stress). (L) A subsection of a full immunoblot shown in fig. S3. Scale bars, 50 μm. Data are presented as means ± SEM except for (B) and (K) (boxplot: interquartile range with whiskers showing minimum to maximum). Statistical significance was assessed by unpaired *t* test (H, J, K, and M), Mann-Whitney test (B and H), or two-way ANOVA with Holm-Sidak correction (D to F and H). $^*P \leq 0.05$, $^{**}P \leq 0.01$, and $^{***}P \leq 0.001$. For detailed statistical information, see tables S1 and S2. See also figs. S1 and S2. Ctr, control; ns, not significant.

of adult metabolism toward energy preservation concomitant with a reduction in the interest for social interactions.

Peripuberty stressed mice show decreased eNAMPT levels and impaired NAD$^+$/SIRT1 pathway in the NAc

Enlargement of adipocytes has been related to adipose tissue dysfunction and a shift in the secretory profile of adipokines (*10*). Therefore, to shed light on the mechanisms linking increased adiposity and impaired sociability, we measured several plasma adipokines. As compared to controls, stressed mice showed a significant decrease on eNAMPT levels (Fig. 1K) but no differences in leptin, adiponectin, FGF-21 (Fibroblast growth factor 21), and Growth Differentiation Factor 15 (GDF-15) (fig. S3, A to D). Consistent with the substantial contribution of adipose tissue to circulating eNAMPT (*13*), eWAT NAMPT protein levels—but not mRNA levels—were reduced in stressed mice (Fig. 1, L and M, and fig. S3, E and F). eNAMPT is enzymatically active and regulates brain NAD$^+$ biosynthesis and SIRT1 activity (*13*). Among several brain regions sensitive to the effects of early life stress (*18*), stressed mice show a specific decline in NAD$^+$ in the NAc (Fig. 2A and fig. S3G). Given the involvement of the NAc in sociability (*17*), we assessed mechanism downstream of NAD$^+$/SIRT1 pathway in this region. In line with the decrease in the levels of NAD$^+$ and its critical role regulating cellular metabolism, stressed mice showed reduced mitochondrial respiration in the NAc (Fig. 2B).

Because of the capacity of SIRT1 to regulate neuronal structure and function (*15*), we next performed ex vivo patch clamp recordings and morphological reconstructions in NAc shell medium spiny neurons (MSNs). MSNs from stressed mice displayed reduced intrinsic excitability (Fig. 2, C to F) and higher rheobase (i.e., the minimal depolarizing current amplitude required to elicit spike discharge) (Fig. 2G), with unaltered threshold potential (Fig. 2H) or dendritic arborization (fig. S3, H and I). Last, expression analysis of SIRT1 target genes related to mitochondrial biogenesis and antioxidant response (*19*) in young adult animals (8 weeks old, not exposed to behavioral testing) revealed a reduction in the expression of *Tfam* (mitochondrial transcription factor), *Nd1* and *Nd6* [subunits of complex I (CI) of the oxidative phosphorylation (OXPHOS)], and *Cat* and *Prx3* (antioxidant enzymes) in the NAc of stressed mice (Fig. 2I). Gene expression levels of *Sirt1*, *Parp1* (NAD$^+$ consumption), or *Nmnat1*, *Nmant2*, and *Nampt* (NAD$^+$ biosynthesis) (*20*) were not affected (fig. S3J). Analysis of SIRT1 gene expression in older animals (32 weeks old, exposed to behavioral testing) revealed a down-regulation of SIRT1 expression in stressed animals (fig. S3K).

The NAD$^+$/SIRT1 pathway in the NAc mediates sociability deficits induced by peripubertal stress

Next, we tested the causal contribution of a blunted NAD$^+$/SIRT1 pathway in the NAc for the sociability changes exhibited by peripuberty stressed mice at adulthood. First, bilateral acute intra-NAc injection of NMN (Fig. 3, A and B)—a NAD$^+$-boosting compound (*11*, *16*)—reverted stress-induced sociability deficits (Fig. 3C and fig. S4A). EX-527 (6-Chloro-2,3,4,9-tetrahydro-1H-carbazole-1-carboxamide), a specific SIRT1 inhibitor (Fig. 3D) (*21*), abolished NMN rescue of sociability (Fig. 3C and fig. S4A). Second, we used two adeno-associated viruses (AAVs) to knock out (Fig. 3, E to H) or overexpress (Fig. 3, I to L) SIRT1 in NAc neurons. SIRT1 knockout mice phenocopied the reduction in sociability exhibited by peripubertally stressed

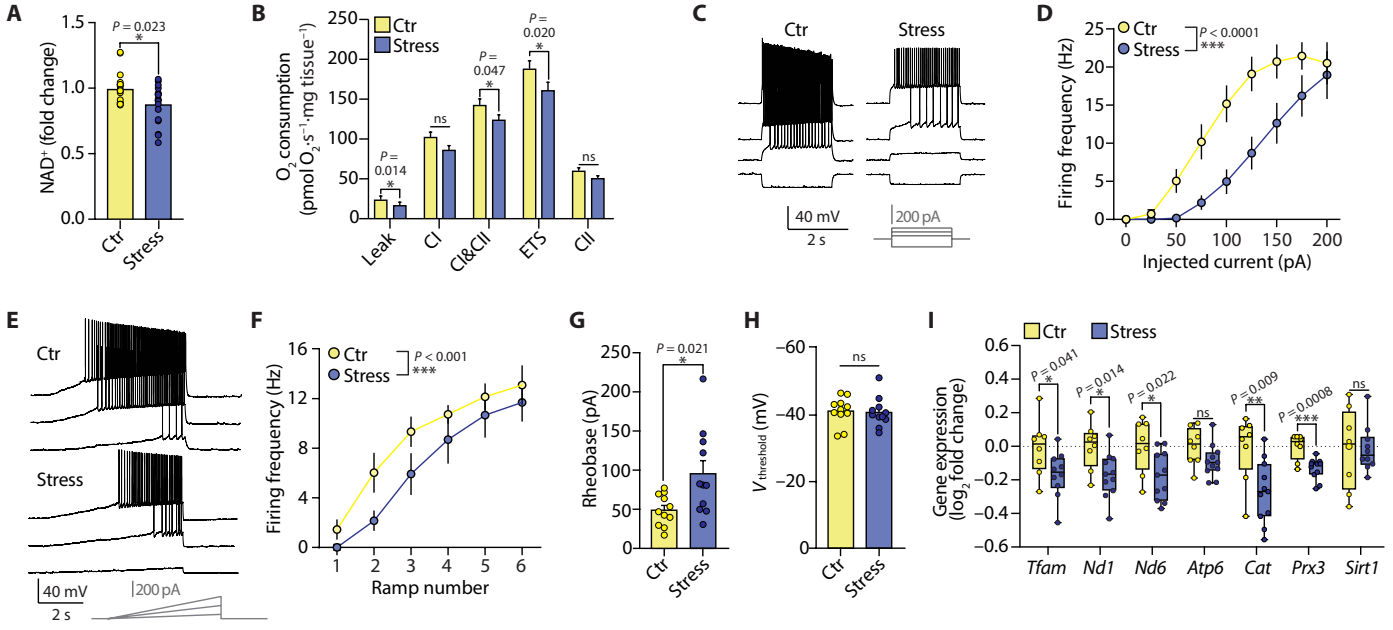

Fig. 2. Adult male mice stressed at peripuberty show impaired NAD$^+$/SIRT1 pathway and reduced MSN excitability in the NAc. NAc of stressed mice exhibited (**A**) decreased levels of NAD$^+$ ($n = 17$ Ctr and 24 Stress) and (**B**) decreased mitochondrial respiration ($n = 11$ Ctr and 11 Stress). (**C** to **H**) Decreased MSN excitability in stressed mice illustrated by (C and E) representative traces of voltage responses, (D) reduced firing frequency to steps of current injection or (F) ramps, and (G) increased rheobase (H) without differences in threshold potential for spike generation ($n = 11$ Ctr and 11 to 12 Stress). (**I**) Decreased expression of SIRT1 target genes in the NAc of stressed mice ($n = 8$ Ctr and 10 to 11 Stress). Data are presented as means ± SEM except for (I) (boxplot: interquartile range with whiskers showing minimum to maximum) and (B) (estimated marginal means ± SEM). Statistical significance was assessed by unpaired *t* test (G and H), Mann-Whitney test (A), linear mixed model (B), or two-way ANOVA with Holm-Sidak correction (D and F). *$P \leq 0.05$, **$P \leq 0.01$, and ***$P \leq 0.001$. For detailed statistical information, see table S3. See also fig. S3.

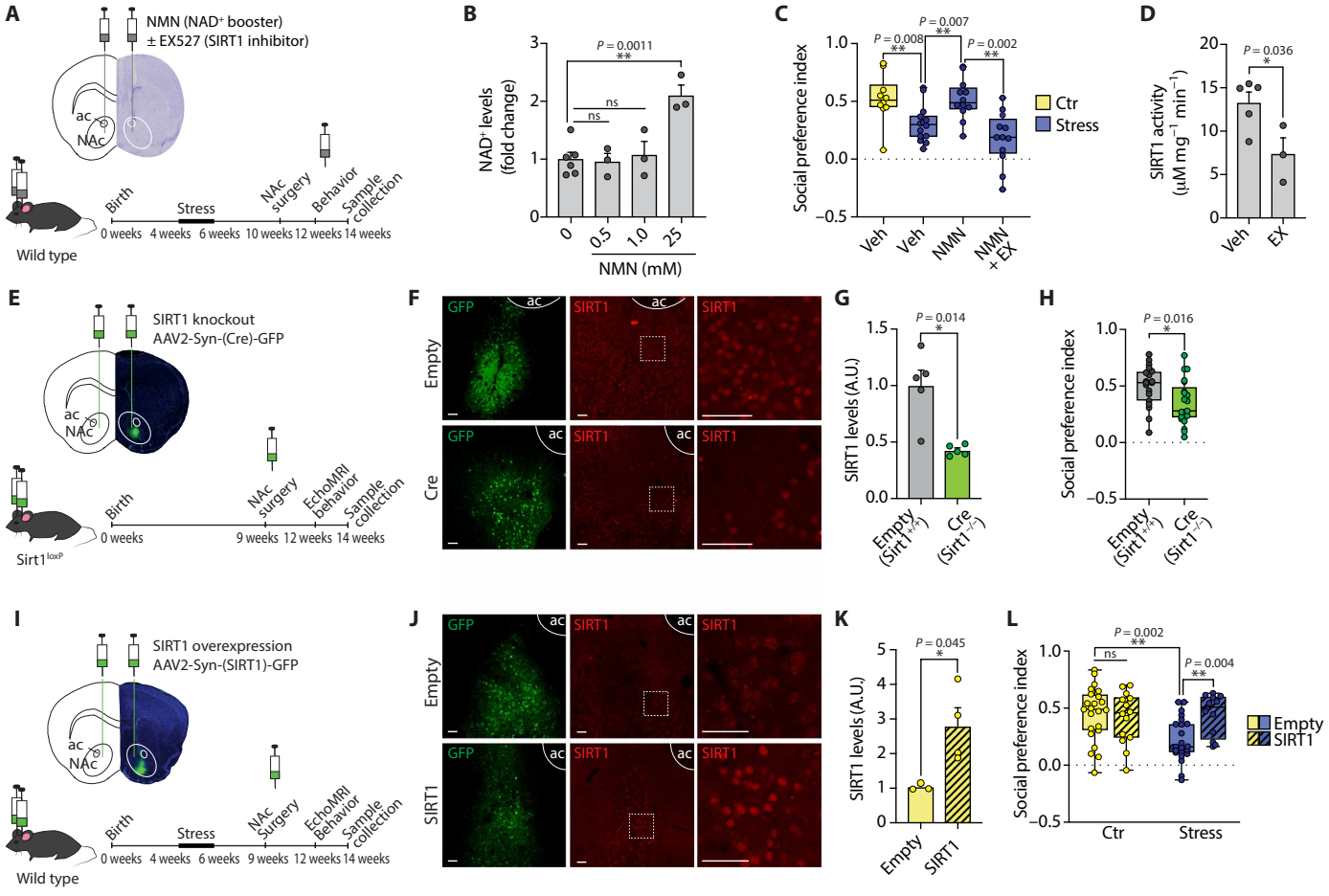

Fig. 3. The NAD+/SIRT1 pathway in the NAc mediates sociability deficits induced by peripubertal stress in male mice. (**A**) Control and stressed mice were implanted with guide cannulas targeted toward the NAc. (**B**) NAc NAD^+ levels in mice injected with vehicle (Veh) or NMN ($n = 3$ to 6). (**C**) Infusion of EX-527 (EX, 0.5 mM) abolished the capacity of NMN (25 mM) to normalize social preference in stressed mice ($n = 10$ Ctr-Veh, 14 Stress-Veh, 12 Stress-NMN, and 12 Stress-NMN-EX). (**D**) Decreased SIRT1 activity in the NAc of mice injected with EX-527 ($n = 5$ Veh and 3 EX). (**E**) *Sirt1*^{loxP} mice were stereotactically injected with AAV2-Syn-GFP (Empty) or AAV2-Syn-Cre-GFP (Cre) in the NAc. (**F** and **G**) Intra-NAc AAV2-Syn-Cre-GFP delivery decreased SIRT1 protein levels measured by immunohistochemistry ($n = 5$ Empty and 5 Cre). (**H**) NAc SIRT1 down-regulation led to decreased social preference ($n = 19$ Empty and 21 Cre). (**I**) Control and stressed mice were stereotactically injected with AAV2-Syn-GFP (Empty) or AAV2-Syn-SIRT1-GFP (SIRT1) in the NAc. (**J** and **K**) AAV2-Syn-SIRT1-GFP achieved SIRT1 overexpression in the NAc measured by immunohistochemistry ($n = 3$ Empty and 4 SIRT1). (**L**) NAc SIRT1 overexpression normalized social preference in stressed mice ($n = 23$ Ctr-Empty, 14 Ctr-SIRT1, 23 Stress-Empty, and 12 Stress-SIRT1). Scale bars, 50 µm. ac, anterior commissure; A.U., arbitrary units. Data are presented as means ± SEM except for (C), (H), and (L) (boxplot: interquartile range with whiskers showing minimum to maximum). Statistical significance was assessed by unpaired *t* test (D, G, H, and K), one-way ANOVA with Holm-Sidak correction (B and C), or two-way ANOVA with Holm-Sidak correction (L). $^*P \leq 0.05$ and $^{**}P \leq 0.01$. For detailed statistical information, see table S4. See also figs. S4 and S5.

mice (Fig. 3H and fig. S4B), while overexpression of SIRT1 in stressed mice rescued their sociability deficits (Fig. 3L and fig. S4C). These results are consistent with the capacity of eNAMPT to activate the NAD^+/SIRT1 pathway in the brain (*13*, *14*, *16*) and support the involvement of this pathway in the NAc mediating the link between decreased circulating eNAMPT and reduced sociability observed in peripubertally stressed mice. Neither NMN nor AAV targeting of SIRT1 in the NAc affected exploratory or anxiety-like behaviors (fig. S4, D to I). Overexpression of SIRT1 (Fig. 3L and fig. S4, C, H, and I) and intra-NAc injections of NMN in control mice (fig. S4, J to M) did not have an impact on sociability or anxiety-like behaviors, despite a significative interaction in the novel object test for the intra-NAc experiment. None of these interventions (i.e., intra-NAc NMN and AAV-mediated SIRT1 overexpression and knockout) altered body weight, body composition, or food intake (figs. S4, N to U, and S5, A to E). Indirect calorimetry measures were not affected in SIRT1 knockout mice either (fig. S5, F to P).

Normalization of eNAMPT levels reduces stress-induced adiposity and reverts alterations in brain function and behavior induced by peripubertal stress through the activation of the NAD^+/SIRT1 pathway in the NAc

To cover the full range of peripubertal stress–induced changes from NAMPT reductions in fat to changes in brain and behavior, we used gene delivery to increase NAMPT expression in adipose tissue (Fig. 4, A and B). Control and stressed adult mice received a recombinant AAV (AS/Rec2) (fig. S6A) that achieves highly selective transduction in visceral fat through intraperitoneal injection (fig. S6, B to H). Both control and stressed mice showed a significant viral transduction in the eWAT (fig. S6, B and C). However,

only stressed mice exhibited increased levels of NAMPT gene expression (mRNA) and protein in eWAT (fig. S6, D to F) and plasma eNAMPT (Fig. 4C). Normalization of plasma eNAMPT levels in stressed mice (Fig. 4C) was accompanied by restoration of NAD^+ levels in the NAc (Fig. 4D) and sociability (Fig. 4, E and F), without changes in anxiety or exploration (fig. S6, K and L). Intrinsic excitability of MSNs in the NAc was also restored (Fig. 4, G to I). In addition, adipose tissue overexpression of NAMPT reduced adiposity—absolute and percentage of fat mass—in stressed mice (fig. S7, A to K). Overexpression of NAMPT in the adipose tissue did not lead to significant differences in gas exchange or energy expenditure during indirect calorimetry studies (fig. S7, L to N). A trend toward a significant interaction effect between stress and NAMPT overexpression was found for the RER (fig. S7O). Food intake (fig. S7P) and levels of leptin, adiponectin, FGF-21, and GDF-15 (fig. S7, R to T) were not affected by the overexpression of NAMPT. Overall, these results show that adipose tissue NAMPT is involved in the alterations of both adiposity and sociability triggered by peripubertal stress (Fig. 4B).

Next, to evaluate whether overexpression of NAMPT in the adipose tissue activated SIRT1 in the NAc, we investigated concomitant changes in the expression of SIRT1 target genes through an orthogonal in situ sequencing (Fig. 5, A to C, and fig. S8, A to E) that allows the analysis of many transcripts with a cellular resolution in one go. Peripubertal stress reduced expression of SIRT1 target genes implicated in mitochondrial biogenesis, dynamics, and respiration—but not genes that regulate neuronal activity—in a multicellular manner (Fig. 5C and fig. S8, A and B). Genes encoding mitochondria

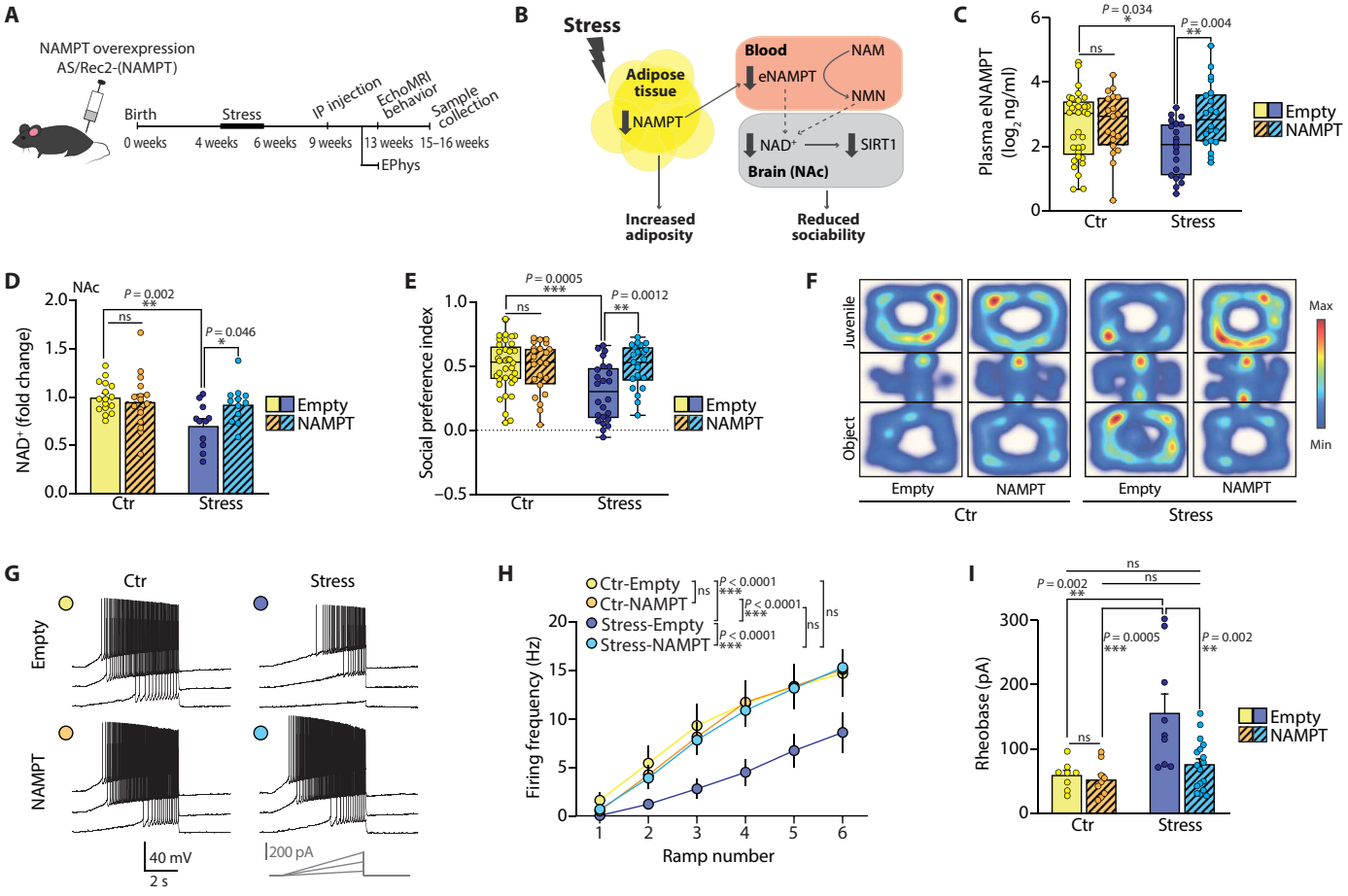

Fig. 4. Normalization of eNAMPT levels reverts alterations in brain function and behavior induced by peripubertal stress in male mice. (**A**) Mice were injected with AS/Rec2-NAMPT (NAMPT) or AS/Rec2-Empty (Empty) virus and either euthanized to perform electrophysiological (EPhys) recordings or subjected to behavioral testing. (**B**) Schematic representation of the eNAMPT signaling pathway upon stress exposure. Stress reduces NAMPT in the adipose tissue and plasma eNAMPT. Decreased NAMPT leads to increased adiposity. Reduced eNAMPT leads to reduced NAD^+ levels in the NAc, impaired SIRT1 function, and reduced sociability. eNAMPT secreted from the adipose tissue converts nicotinamide (NAM) into NMN, which is converted into NAD^+ and activates SIRT1. (**C**) AS/Rec2-NAMPT injection normalized eNAMPT levels in stressed mice ($n = 32$ Ctr-Empty, 19 Ctr-NAMPT, 20 Stress-Empty, and 20 Stress-NAMPT) and (**D**) NAD^+ levels in the NAc ($n = 16$ Ctr-Empty, 16 Ctr-NAMPT, 11 Stress-Empty, and 12 Stress-NAMPT). (**E** and **F**) Increased plasma eNAMPT normalized sociability in stressed mice ($n = 36$ Ctr-Empty, 23 Ctr-NAMPT, 24 Stress-Empty, and 22 Stress-NAMPT) and representative heatmaps of mouse position during the social preference test. (**G** to **I**) (G) Representative traces of voltage responses showing that (H) AS/Rec2-NAMPT injection in stressed mice normalized evoked firing ($n = 9$ Ctr-Empty, 10 Ctr-NAMPT, 9 Stress-Empty, and 18 Stress-NAMPT) (I) and rheobase values in MSNs of the NAc ($n = 8$ Ctr-Empty, 9 Ctr-NAMPT, 9 Stress-Empty, and 17 Stress-NAMPT). Data are presented as means ± SEM except for (C) and (E) (boxplot: interquartile range with whiskers showing minimum to maximum). Statistical significance was assessed by two-way ANOVA with Holm-Sidak correction (C to E and H), or one-way ANOVA with Holm-Sidak correction (I). $^*P \leq 0.05$, $^{**}P \leq 0.01$, and $^{***}P \leq 0.001$. For detailed statistical information, see table S5. See also figs. S6 and S7.

complex subunits (e.g., *Shda*, *Uqcrb*, *Nd1*, and *Atp6*) (*19*) were down-regulated in D1- and D2-MSNs, as well as in astrocytes and microglia. Other SIRT1 target genes were, however, down-regulated in a cell type–specific manner, such as *Bnip3* and *Cs* in D2-MSNs or *Aco2* (*19*, *22*) in astrocytes. Normalization of eNAMPT levels up-regulated the expression of mitochondrial genes that were down-regulated by peripubertal stress (Fig. 5C and fig. S8, A and B). These findings further support the hypothesis that normalization of adipose tissue NAMPT levels and, consequently, eNAMPT plasma levels mediates the behavioral improvement in stressed mice via activation of the SIRT1 pathway in the NAc.

Dietary supplementation with NMN reverts the alterations in brain function and behavior induced by peripubertal stress

Last, aiming at a translational application, we evaluated the therapeutic potential of systemic treatment with NMN in stressed mice. NAD^+ levels in the brain have been shown to increase 15 min after an intraperitoneal injection of NMN, suggesting that NMN is able to cross the blood-brain barrier (BBB) (*16*). Dietary supplementation of NMN has been successfully used to correct imbalances in NAD^+ metabolism and behavior in animal models of ataxia and cerebral ischemia (*16*). In our study, administration of NMN for 2.5 weeks

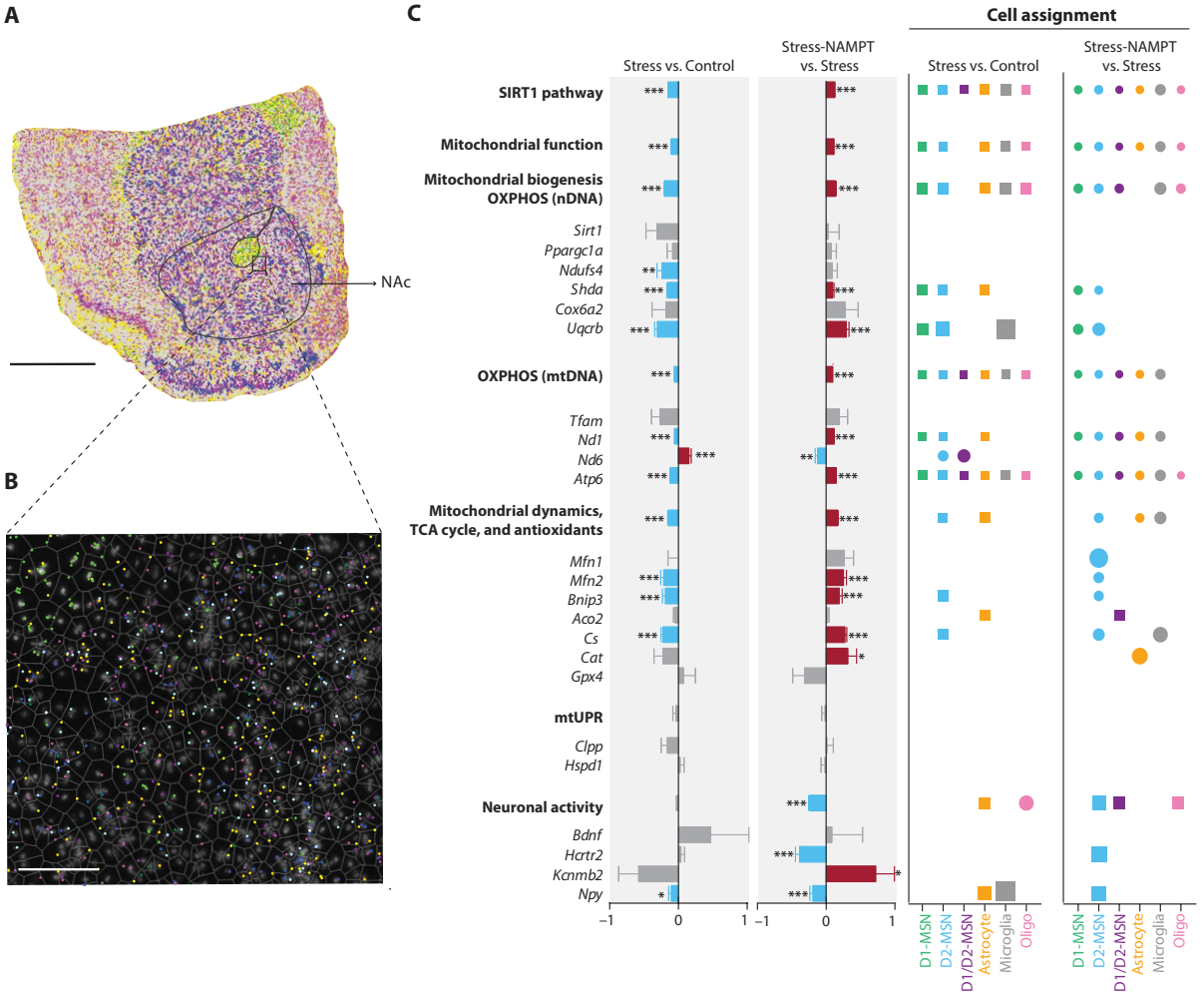

Fig. 5. Normalization of eNAMPT levels promotes the expression of SIRT1 target genes in the NAc of adult male mice stressed at peripuberty. (**A**) Representative image of in situ sequencing showing the distribution of 33 genes (SIRT1-targets and cell specific-type marker) in a mice brain coronal section indicating the NAc. (**B**) Magnification showing cell segmentation (white lines) and gene reads of representative cell-type markers [D1-MSNs (*Drd1*, dark blue), D2-MSNs (*Drd2*, purple), astrocytes (*Aqp4*, gray), microglia (*Ctss*, dark gray), and oligodendrocytes (*Plp*, green)] and SIRT1-targets [*Uqcrb* (pink), *Nd6* (yellow), *Mfn2* (light blue), *Hspd1* (orange), and *Hcrtr2* (dark green)]. Scale bar, 1 mm (A), 100 μm (B). (**C**) Expression analysis of SIRT1 target genes (in italics) or composite score (in bold) in the NAc between stressed and control mice injected with AS/Rec2-Empty and stressed mice injected with AS/Rec2-NAMPT or the AS/Rec2-Empty and represented by the fixed-effect estimate of each group comparison on each gene/composite score (negative value, decreased expression; positive value, increased expression) ($n = 3$ Ctr-Empty, 3 Stress-Empty, and 4 Stress-NAMPT). The "cell assignment" columns represent the analysis of each gene/composite score in a particular cell type (round shape, positive estimate; square shape, negative estimate; shape size, proportional to the fixed-effect estimate). Only significant values ($P \leq 0.05$) are shown in the cell assignment plots. Oligo, oligodendrocytes. Data are presented as fixed-effect estimates ± SE. Statistical significance was assessed using a generalized linear mixed-effects model with FDR correction. $^*P \leq 0.05$, $^{**}P \leq 0.01$, and $^{***}P \leq 0.001$. For detailed statistical information, see table S6. See also fig. S8.

in the drinking water (Fig. 6A) mimicked the results obtained when normalizing eNAMPT levels in stressed mice on brain function and behavior: reverting sociability alterations (Fig. 6, B and C, and fig. S9, A to C), as well as the stress-induced decline in NAc NAD^+ levels (Fig. 6D) and changes in NAc MSNs excitability (Fig. 6, E to G). However, adiposity and food intake were not reverted in stressed mice treated with NMN (fig. S9, D to I). These results highlight an unexpected potential of dietary supplementation with NMN to revert the alterations induced by peripubertal stress in NAc function and social behavior.

DISCUSSION

Here, we identify a critical role for NAMPT as a key effector of an adipose-to-brain signaling pathway that sustains the association between increased adiposity and impaired sociability triggered by early life stress. Social interactions are at the core of individuals' well-being and the functioning of societies. In humans, reductions in sociability, e.g., social avoidance or withdrawal, can be manifestations of a broad range of psychopathologies (*23*). Despite the detrimental impact of social dysfunctions for both the individual and society, the underlying mechanisms are unclear and effective treatments are lacking. Here, we contribute a novel mouse model that recapitulates the association between increased adiposity and impaired sociability and provide a mechanistic understanding of how changes in eNAMPT alter NAD^+/SIRT1 signaling in the NAc to modify social behavior in male mice. We also provide a proof of principle that targeting adipose NAMPT levels and systemically administering NMN are promising opportunities to revert behavioral deficits of early life stress origin.

Obesity, defined as excess accumulation of WAT, is associated with increased risk for developing a broad range of health problems (*2*). In humans, obesity and deficits in the social domain are frequently found interrelated (*7*, *8*). However, to what extent obesity-associated social withdrawal can be explained by behavioral changes in the overweight individual and whether metabolic factors can explain social deficits are not well understood and difficult to tackle. Here, we provide a mouse model that shows in male—but not in female—animals an association between increased adiposity and sociability deficits frequently reported in humans, allowing us to investigate the mechanistic underpinnings of this association. Previous clinical and preclinical work had shown that stress exposure during childhood and adolescence can trigger increased adiposity and obesity (*5*, *6*, *24*) and reduced sociability (*3*, *25*) over the life course. However, each of these independent studies focused on their respective domains, and alterations in adiposity and sociability were never reported concomitantly. Thus, a key strength of our model is that both behavioral and metabolic adaptations are simultaneously observed, indicating that this comorbidity can represent a common biological embedding triggered by early life adversity.

Similar to humans (*26*), adipose tissue cellularity in mice is set at peripuberty—a critical period of adipose tissue maturation and proliferation (*2*). Accordingly, foundations for excessive adiposity are laid down during the peripubertal period (*27*). Our findings show that adult mice stressed during the peripubertal period exhibit a higher percentage of fat mass and adipocyte hypertrophy. Although

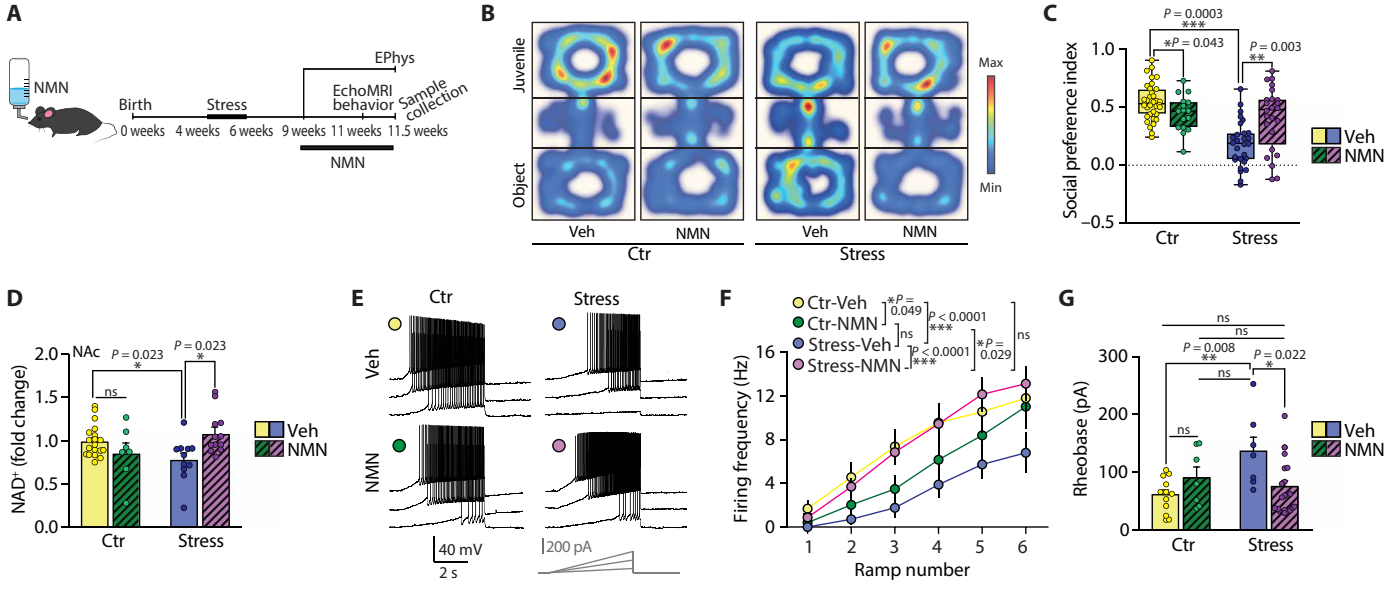

Fig. 6. Dietary supplementation with NMN reverts the alterations in brain function and behavior induced by peripubertal stress in adult male mice. (**A**) Mice were treated with NMN (100 mg/kg per day) for 2.5 weeks and euthanized to perform EPhys recordings or subjected to behavioral testing. (**B** and **C**) Representative heatmaps of mouse position during the social preference test illustrating that decreased sociability is normalized in stressed mice treated with NMN ($n = 35$ Ctr, 16 Ctr-NMN, 28 Stress, and 14 Stress-NMN). (**D**) NMN treatment restored NAD^+ levels in the NAc ($n = 19$ Ctr, 7 Ctr-NMN, 11 Stress, and 12 Stress-NMN). (**E** to **G**) (E) Representative traces of voltage responses showing that (F) NMN treatment restored evoked firing ($n = 13$ Ctr, 7 Ctr-NMN, 7 Stress, and 21 Stress-NMN) (G) and rheobase values ($n = 12$ Ctr, 7 Ctr-NMN, 7 Stress, and 21 Stress-NMN) in MSN in stressed mice. Data are presented as means ± SEM except for (C) (boxplot: interquartile range with whiskers showing minimum to maximum). Statistical significance was assessed by two-way ANOVA with Holm-Sidak correction (C, D, and F) or one-way ANOVA with Holm-Sidak correction (G). $*P \leq 0.05$, $**P \leq 0.01$, and $***P \leq 0.001$. For detailed statistical information, see table S7. See also fig. S9.

our mice were maintained under a normal diet, they developed an obesogenic phenotype characterized by reduced lean mass and increased fat mass—without changes in body weight—in parallel to an enlargement of adipocytes and reduced food intake, mild glucose intolerance, and reduced RER. These findings indicate that peripuberty stress reprograms adult metabolism toward storage of energy in the adipose tissue and is consistent with the view that early life stress leads to increased metabolic vulnerability (*28*). According to the cumulative stress hypothesis (*29*), exposure to a second hit, such as high-caloric diets or other environmental stressors, could unravel metabolic abnormalities (e.g., expected reduced energy expenditure in animals that show reduced food intake) or aggravate other metabolic parameters (e.g., body weight increase and insulin resistance) that are imperceptible after the first hit.

The modulation of metabolism by adipokines is rather well established (*10*); however, much less is known about their actions in brain function and behaviors not directly linked to energy homeostasis. Although a reduction in plasma adiponectin levels was previously linked to decreased sociability (*30*), the brain effector mechanisms of this phenomenon were not unveiled. Here, we show that peripubertally stressed mice display a specific decrease in the circulating levels of the eNAMPT (levels of leptin, adiponectin, FGF-21, and GDF-15 were unchanged), along with diminished NAMPT protein levels in adipose tissue. Previous studies reported that obese mice—as a consequence of consuming a high-fat diet—show decreased NAMPT levels in the adipose tissue (*31*, *32*). Our results demonstrate that this phenomenon is observed in obesity triggered by early life stress in mice. To date, studies linking obesity with adipose tissue NAMPT and plasma eNAMPT in humans are inconclusive. Some studies in obese populations showed reduced levels of NAMPT in the adipose tissue (*33*) and reduced plasma eNAMPT (*34*). There is also evidence, however, of increased eNAMPT levels in patients with obesity (*35*) and a positive (but weak) correlation between adipose tissue NAMPT expression and adiposity and eNAMPT (*36*). Nevertheless, in some reports, increased eNAMPT was only observed in patients with severe obesity accompanied with an impaired glucose tolerance (*37*), and a multiple regression analysis determined that increased eNAMPT levels in patients with type 2 diabetes is independent of obesity and is mainly determined by triglycerides and fasting glucose levels (*38*). Overall, the relationship between eNAMPT and obesity in humans is far from being understood, and including other mediators to the equation, such as exposure to early life stress, might shed some light to this question. Circulating eNAMPT can be internalized in the brain, as previously shown for the hypothalamus where it promotes the synthesis of NMN/NAD^+ and the consequent activation of the NAD^+-dependent protein deacetylase SIRT1 (*13*, *14*, *16*). In our study, adult mice submitted to peripubertal stress exhibit reduced NAD^+ levels specifically in the NAc—a brain region critically involved in the regulation of social motivation (*17*)—but not in several other brain regions analyzed (i.e., hypothalamic arcuate nucleus, the ventral tegmental area, or the basolateral amygdala). Analysis of NAD^+ levels in the ventromedial nucleus of the hypothalamus—a brain region that regulates aggression (*39*)—did not reveal differences between control and stress mice either. These results are aligned with the absence of changes in aggressive behavior in peripubertal stress mice and suggest that the stress-induced alterations in eNAMPT have a particular selectivity for the NAc. The NAc is one of the brain regions whose integrity is sensitive to stress exposure (*18*, *40*), and recent evidence shows its prominent vulnerability to develop neurovascular alterations involving increased BBB permeability following stress exposure (*41*). This sensitivity may explain the link between reduced plasma eNAMPT and the accumbal NAD^+ reduction that we observe in peripubertally stressed mice.

In addition, congruent with the accumbal NAD^+ reduction, young adult mice submitted to peripubertal stress also exhibit reductions in the expression of SIRT1 target genes and decreased mitochondrial function. Changes in SIRT1 gene expression showed a temporal pattern: unaltered expression levels in 8-week-old stressed mice but decreased expression level in older (32-week-old) stressed mice. This time-dependent regulation of SIRT1 expression could be mediated by the SIRT1-FOXO positive feedback loop, in which SIRT1 deacetylates and activates FOXO, leading to a FOXO-dependent transcription of SIRT1 (*42*). Therefore, impaired SIRT1 activity—triggered by diminished NAD^+ levels—would eventually lead to a reduced expression of SIRT1. A previous study showed increased accumbal SIRT1 expression following chronic social defeat stress in adult mice (*21*), suggesting a differential regulation of this pathway by early life and adult stressors. This possibility is in agreement with time-dependent SIRT1 regulation under stress conditions described in cell lines (*43*). On the other hand, the reduction in mitochondria respiration aligns well with the recent involvement of mitochondrial function in the NAc in the regulation of social behaviors (*44*–*46*).

We additionally found that the abovementioned alterations are accompanied by a decrease in the intrinsic excitability of accumbal MSNs. The limited engagement of NAc neurons is consistent with the decreased sociability of peripubertally stressed mice, as exploration of a social target is associated with increased NAc neuronal spiking (*47*). Previous studies addressing the impact of chronic social defeat in mice indicate that D1-MSNs from stress-exposed mice exhibit alterations in intrinsic excitability as a result of morphological changes that affect cell input resistance (*48*). As we found no morphological changes in MSNs from peripubertally stressed mice, the decreased excitability is likely to be caused by ionic mechanisms that impinge on action potential generation and repetitive firing. On the one hand, neuronal firing is tightly coupled to mitochondrial function, as action potential generation depends on adenosine 5′-triphosphate (ATP) levels and spike threshold is regulated by ATP-dependent potassium conductances (*49*). On the other hand, as confirmed by our data, SIRT1 regulates the expression of *Kcnmb2* (*50*), which encodes for the β_2 subunit of the large-conductance calcium- and voltage-activated potassium (BK) channels. The β_2 subunit rapidly inactivates BK channels, thereby promoting intrinsic excitability. Thus, the decreased excitability found in MSNs from peripubertally stressed mice may result from a concomitant decrease in ATP levels and increase in potassium conductances.

We implicated the NAD^+/SIRT1 pathway in the NAc in the sociability deficit induced by peripubertal stress through three complementary experiments with targeted accumbal interventions. First, we showed that administration of NMN—an NAD^+ booster that regulates SIRT1 activity (*16*)—in the NAc reverts the stress-induced behavioral phenotype, while coinjection with a SIRT1 inhibitor abolishes the effect. These results align with the observation that intra-accumbal infusion of nicotinamide, a precursor of NMN, prevents the development of a subordinate status in highly anxious rats (*45*), and confirm that NMN in the NAc acts in a SIRT1-dependent manner. Then, we showed that virally-mediated down-regulation of SIRT1 expression in the NAc leads to social deficits, mimicking the

peripubertal stress–induced adult phenotype. Last, we established causality of the SIRT1 pathway by showing that viral-induced SIRT1 overexpression in the NAc rescues the peripubertal stress–induced behavioral phenotype.

Furthermore, virally induced overexpression of NAMPT in adipose tissue was a critical approach in our study to causally implicate the observed NAMPT reduction on the protracted peripubertal stress–related effects at both the behavioral and the accumbal neurometabolic levels. Adipose NAMPT overexpression at adulthood normalized peripuberty stress–induced impairments in (i) plasma eNAMPT levels, (ii) accumbal NAD^+ content, (iii) accumbal MSNs' intrinsic excitability, and (iv) social behavior. These results align with previous studies that showed increased NAD^+ levels in hypothalamic explants cultured in media supplemented with purified eNAMPT and in the hypothalamus of adipose tissue–specific constitutive NAMPT knock-in mice (*13*, *14*). They also expand the capacity of circulating eNAMPT to influence NAD^+ in the NAc of stressed animals. In addition, adipose tissue NAMPT overexpression decreased stress-induced adiposity. Whereas overexpression of NAMPT in the adipose tissue leads to both a reduction in adiposity and a complete rescue of the sociability deficits, interventions that activate the pathways downstream of adipose tissue NAMPT, such as systemic NMN treatment or direct targeting of SIRT1 in the NAc, did not have an impact on body composition. These observations were essential to understand the directionality of the signaling pathway: NAMPT in the adipose tissue is the most upstream element of the pathway, involved in the stress-induced changes in adiposity and sociability; eNAMPT/NMN mediates the communication of the adipose tissue with the NAc; and, lastly, SIRT1 in the NAc is the downstream effector in this signaling pathway that regulates sociability (Fig. 4B).

Gene expression analyses by CARTANA in situ sequencing revealed that genes of the SIRT1 pathway—particularly genes involved in the regulation of mitochondrial function—are down-regulated in the NAc of stressed mice and that normalization of eNAMPT was sufficient to increase the expression of these genes. Mitochondrial function is essential to support neuronal excitability (*51*) and increasing evidence point at mitochondria in the etiology of stress-induced psychiatric disorders (*52*). Particularly in the NAc, variations in mitochondrial function (*45*, *46*) and metabolism (*53*–*55*) are related to differences in anxiety, depression-like behaviors, and social competitiveness. In addition, a previous report suggested an impaired SIRT1 pathway in the brain of mice exposed to maternal deprivation (*56*). We observed that stressed mice show a down-regulation in subunits of the OXPHOS system encoded by the nuclear (*Shda* and *Uqcrb*) and the mitochondrial DNA (*Nd1* and *Atp6*) together with genes involved in the tricarboxylic acid (TCA) cycle (*Cs*), mitochondrial fusion (*Mfn2*), and mitophagy (*Bnip3*). The expression of these genes was increased in stressed mice injected with a viral vector system to overexpress NAMPT specifically in adipose tissue. NAD^+ replenishment and SIRT1 activation also prevent brain aging and neurodegenerative disease via activation of mitochondrial function, mitochondrial biogenesis, and mitophagy (*12*), and MFN2 in the NAc has recently been implicated in the depression-like behavior exhibited by highly anxious rats (*44*). On the other hand, stress during peripuberty did not induce changes in other SIRT1 targets including mitochondrial unfolded protein response (mtUPR)–related genes (*12*) and genes implicated in neuronal function and plasticity such as *Hcrtr2* (*50*), *Kcnmb2* (*50*), and *Bdnf* (*22*). We observed, however, that overexpression of eNAMPT in stressed mice promotes the expression of *Kcnmb2*, which is also increased in the hypothalamus of brain-specific SIRT1-overexpressing transgenic mice (*50*). The cellular resolution provided by our in situ sequencing experiment revealed that, while OXPHOS subunits are down-regulated in a multicellular manner, the expression of genes related to mitochondrial dynamics such as *Mfn2* (in the NAc shell) and *Bnip3* is significantly decreased in D2-MSN. A recent report shows that D2-MSN show more frequently shorter mitochondria in dendrites, while D1-MSN dendrites exhibit longer mitochondria (*57*), suggesting distinct patterns of mitochondrial dynamics regulation in these two types of neurons.

Last, aiming at a translational application, we evaluated the therapeutic potential of a nutritional intervention with NMN to revert symptomatology observed at adulthood in peripuberty stressed mice. In line with the results obtained with the virally induced overexpression of NAMPT in adipose tissue (see above), NMN treatment normalized stress-induced reductions in (i) accumbal NAD^+ content, (ii) accumbal MSNs' intrinsic excitability, and (iii) social behavior. NAD intermediates, such as NMN and nicotinamide riboside (NR), have been used as effective nutraceuticals to mitigate age-related physiological decline and increase body's resilience to disease in several mouse models (*16*). For instance, a defect in physical activity observed in NAMPT knockout mice was ameliorated by NMN treatment (*13*). In clinical trials, treatment with EH301 (a derivate of NR) significantly slowed disease progression in patients with amyotrophic lateral sclerosis (*58*). Moreover, a recent clinical trial demonstrated that oral administration of NMN is safe and effectively metabolized in healthy men (*59*). Small molecules acting as NAMPT activators are emerging as promising tools to catalyze NMN production and may be interesting for future interventions (*60*).

An intriguing question is why does increasing NAMPT in adipose tissue or activating SIRT1 pathway in the NAc trigger different responses in control and stressed mice, i.e., rescue of sociability deficits in stressed mice, while there are no changes found, or even the opposite pattern is observed, in control mice. These results suggest that the NAc might have mechanisms that avoid SIRT1 overactivation, which could lead to excessive mitochondrial respiration and, eventually, to oxidative damage. In addition, systemic treatment with NMN for 2.5 weeks led to a reduction in sociability and intrinsic excitability. These effects could be explained by time-dependent changes on the response to NMN eventually involving the activation of poly[adenosine 5′-diphosphate (ADP)–ribose)] polymerase (PARP) proteins, NAD^+-consuming enzymes that inhibit SIRT1 activity and expression (*61*). Another study showed a similar paradoxical response pattern to NMN in the context of cocaine treatment (*62*). Last, in control animals injected with the AS/Rec2-NAMPT virus, NAMPT expression was not up-regulated at the long-term time point at which samples were collected, despite the fact that both control and stressed animals showed significant viral transduction in the adipose tissue. These results are consistent with an early expression of NAMPT followed by an eventual silencing mediated by the activation of homeostatic mechanisms such as the UPR (*63*).

Our findings resonate with reports indicating age-related reductions in both eNAMPT circulating levels (*14*) and brain NAD^+ content (*12*), aligning with the view that stress accelerates biological aging (*64*). They may also have implications to understand key features of depression. Decreased sociability is a prominent manifestation of

depression (*65*) and depression is consistently reported for individuals that experienced adversity around childhood and adolescence (*4*). The odds of developing depression are higher in obese individuals and genetic studies indicate a causal relationship between obesity, and particularly fat mass increase, and the likelihood to develop depression (*66*). In our study, the use of an inbred mouse strain (C57BL/6J), devoid of genetic variability, allows revealing peripubertal stress as an important risk factor for the development of this combined metabolic and behavioral phenotype. Compared to the CUS protocol, a model classically used to study depression (*67*, *68*), our model of unpredictable stress during peripuberty does not show anhedonia, in line with our previous work in rats exposed to peripubertal stress (*69*). These differences can be explained by the different duration of the stress protocol, the type of stressors used, and the time window of stress exposure. First, the peripubertal stress protocol consists of 7 days of stress exposure scattered over a period of 14 days. On the contrary, CUS involves exposure to daily stressors, lasting for at least 4 weeks (up to 8 weeks in some studies) (*68*). Second, the nature of the stressors differs between protocols: While only physical and innate stressors are used in the peripubertal stress procedure, CUS protocols typically include water and/or food deprivation, changes in light-dark cycle, and stressors of social nature (e.g., cage crowding and social defeat) (*68*). Last, CUS is generally used in studies that investigate the "immediate" impact of stress exposure at adulthood, while our peripubertal stress protocol was designed to study the "long-term" consequences of stress exposure at peripuberty (*68*). Stress exposure during this sensitive early time period has been shown to have a profound impact on social behavior in both rodents and humans (*3*).

Because of the long length of each peripubertal stress study with analyses at adulthood and the lack of a prominent phenotype in stressed female mice, this work has focused on the phenomenon and dissection of the mechanisms involved only in males. However, a limitation of this study is that we cannot extrapolate whether the eNAMPT/SIRT1 pathway has an impact on brain function or in other behaviors (e.g., maternal care) not explored in female mice. Another question that remains open is the precise molecular mechanisms whereby early life stress induces a reduction in eNAMPT. Glucocorticoids—the main hormone from the hypothalamic-pituitary-adrenal axis secreted in response to stress—are prominent regulators of adipose tissue metabolism (*70*), and the *Nampt* gene contains several glucocorticoid regulatory elements in its promoter (*71*). In addition, dexamethasone—a synthetic glucocorticoid—increases NAMPT expression in 3T3-L1 adipocytes (*72*). Further research is thus warranted to elucidate whether stress-induced alterations in eNAMPT levels are mediated by glucocorticoids. Moreover, our data point to the NAc as the brain region that drives the sociability alterations present in peripuberty stress mice. Although we did not find stress-induced NAD^+ changes in other brain regions analyzed, we cannot completely rule out that impaired eNAMPT signaling is affecting other organs, brain regions, or behaviors not explored in this work. Last, housing conditions in indirect calorimetry cages differ considerably from the standard cages (i.e., single housing, smaller cages, absence of nesting and hiding material, new feeding, and drinking system). Habituation time and metabolic responses to this novel environment might diverge between control and stressed animals (*73*).

Overall, our study supports the view that early life stress can lead to enduring changes in biological and developmental systems (i.e., biological embedding) that affect health and behavior over the life course (*74*). The metabolic and behavioral phenotype displayed by peripuberty stressed mice aligns well with an evolutionary developmental perspective that considers that early stress may prompt the development of costly but adaptive enduring strategies that promote survival and reproduction under stressful conditions (*74*). The phenotypic changes observed in peripuberty stressed mice can be interpreted as developmental adaptations in preparation for future demanding conditions (*74*). Different noncompeting mechanisms may operate during peripubertal stress exposure toward the programmed phenotype: (i) the reduction in body weight induced by the activation of physiological stress during the period of unpredictable stress exposure (*75*) and (ii) the lack of food availability in the threatening contexts may reinforce the development of an adaptation to save energy resources for potential future scarcity. Natural selection favors organisms that schedule developmental activities so as to optimize resource allocation (*74*) and most stressors regulate metabolic processes to compensate for stress demands by conserving adipose tissue (*75*).

In conclusion, we uncover a fat-to-brain pathway that mediates the association between increased adiposity and sociability deficits observed in adult individuals submitted to stress during the peripubertal period. We identify fat NAMPT as a triggering mechanism that involves reduced circulating eNAMPT levels and concomitant reductions in NAD^+/SIRT1 signaling in the NAc, and we implicate these changes in protracted effects of stress in social behavior. Last, we highlight NAD^+ boosters as a promising strategy to revert behavioral deficits associated with alterations in fat metabolism, particularly if triggered by early life stress.

MATERIALS AND METHODS

Animals

Experimental male and female mice were the offspring of C57BL/6J mice bred in our animal facility. Breeding pairs were purchased from a commercial breeder (Charles River Laboratories, France) and acclimated in our animal facility upon arrival. Behavioral testing, metabolic assessment, molecular analysis, and electrophysiological recordings were performed in adult male mice aged 8 to 16 weeks. Mice from the same home cage were always assigned to the same experimental group. *Sirt1*^{loxP} mice (on a pure C57BL/6J background) were provided by J.A. (*76*). Juvenile C57BL/6J male mice (3 weeks old) for the social preference test, CD1 male old breeders for the social interaction test, and socially experienced adult BALB/c male mice for the resident intruder test were purchased from a commercial breeder (Charles River Laboratories, France) and acclimated in our animal facility upon arrival at least 1 week before the behavioral testing. Food and water were available ad libitum. Mice were maintained under standard housing conditions on a 12-hour light/12-hour dark cycle (lights on at 7:00 a.m.). All experiments were performed with the approval of the Cantonal Veterinary Authorities (Vaud, Switzerland) and carried out in accordance with the European Communities Council Directive of 22 September 2010 (2010/63/EU).

Peripubertal stress

The peripubertal stress paradigm aims to model exposure to unpredictable stressful experiences of nonsocial nature during late childhood and puberty. At postnatal day 21 (PN21), mice were weaned

and four male mice from different litters were assigned into a new home cage. At PN27, cages were assigned to either the experimental group "control" (Ctr) or the experimental group "Stress," after being counterbalanced by body weight and body composition (EchoMRI). On seven scattered days between the PN28 and the PN42, animals from the Stress group were exposed to innate and physical stressors in a repetitive but unpredictable manner. Stressors were applied in two sessions—morning (a.m.) and afternoon (p.m.)—separated by a resting period of minimum 3 hours. PN28 (a.m.): Mice were placed in the open field (a rectangular arena of 50 cm by 50 cm) for 5 min. Immediately after, animals were transferred to an elevated platform (EP) (a 12 cm–by–12 cm platform elevated 95 cm from the ground) under direct bright light (470 to 500 lux) for 25 min. After the exposure to the EP, a small incision was made on the distal part of the tail with the help of a blade. Blood was collected through a pre-heparinized capillary immediately after the exposure to EP ($t_{0'}$) and 30 min later ($t_{30'}$). PN28 (p.m.): Mice were immobilized with a restrainer for 30 min. PN29 (a.m.): During 10 min, mice were subjected to the tail suspension test (TST), in which mice were suspended by the tail from a tube placed 10 cm away from the ground. PN29 (p.m.): Mice were placed inside a plastic box (38 cm by 27.5 cm by 31 cm) for 30 min under a bright light (210 to 250 lux) and exposed to the synthetic fox odor 2,4,5-trimethylthiazole (TMT) (Sigma-Aldrich, #W332518) through a small cloth. Immediately after, animals were transferred to the EP for 25 min, and blood was obtained at $t_{0'}$ and $t_{30'}$ as described above. PN30 (a.m.): Mice were placed in the EP for 25 min followed by exposition to TMT for 25 min. Blood was obtained at $t_{0'}$ and $t_{30'}$. PN30 (p.m.): Mice were immobilized with a restrainer for 30 min. PN34 (a.m.): Mice were exposed to TMT for 25 min. PN34 (p.m.): Mice were subjected to the TST for 10 min followed by 30 min of immobilization with a restrainer. PN36 (a.m.): Mice were immobilized with a restrainer for 30 min. Thereafter, mice were subjected to the forced swim test (FST). In this test, mice were placed 10 min inside a glass beaker (25 cm tall by 14 cm diameter) containing water at 23° to 25°C. PN36 (p.m.): Mice were placed on the EP for 25 min. PN40 (a.m.): Mice were placed on the EP for 25 min followed by exposition to TMT for 25 min. PN40 (p.m.): Mice were subjected to the FST for 10 min. PN42 (a.m.): Mice were immobilized with a restrainer for 30 min followed by 10 min of FST. PN42 (p.m.): Mice were placed on the EP for 25 min, and blood was obtained at $t_{0'}$ and $t_{30'}$. Control animals were handled the same days that their counterparts were exposed to stress. Body weight and food intake by cage were monitored every day of the stress protocol (Stress group) or during the handling (Ctr group).

Animal behavior

Social preference test

This test assesses animals' preference to explore either a social conspecific of the same sex or an inanimate object. The arena consists of a rectangular, three-chambered box with a center compartment (20 cm by 35 cm by 35 cm) and two side compartments (30 cm by 35 cm by 35 cm) made of gray polyvinyl chloride. Dividing walls with retractable doorways were located between the compartments to allow or prevent access to the side chambers. In both side chambers, a wire cage (10.16 cm bottom diameter, 11 cm high, bars spaced 0.5 cm apart, made of chrome, Kitchen Plus Galaxy Pencil & Utility cup) was located to prevent any type of direct physical contact, thereby still allowing olfactory contact and social approach to the respective stimulus enclosed in the wire cage. Every experimental animal was put in the center compartment with both doors closed to habituate to the apparatus for 5 min. The doors were then opened, and the animal was allowed to explore the whole apparatus for 10 min, with the side chambers containing either an object (black dummy mouse) or a juvenile C57BL/6J (28 ± 2 days), respectively. Light conditions were kept at 2 to 3 lux with homogeneous illumination in the chambers. The apparatus floor was covered with sawdust. Two consecutive days before testing, animals were habituated to the apparatus for 10 min, and juvenile mice were habituated to the cylinders for a minimum of 30 min. The time spent sniffing each wire cage was video-recorded and manually scored by an experienced researcher blinded to the experimental group to evaluate the level of preference for the unfamiliar mouse compared with the object using an in-house software [Clicker, Ecole Polytechnique Fédérale de Lausanne (EPFL)]. The social preference ratio was calculated according to the following formula: (time sniffing the juvenile – time sniffing the object)/(total sniffing time). Representative heatmaps of the mouse position during the three-chamber social preference test were obtained with EthoVision (Noldus Information Technology).

Elevated plus maze test

The maze consists of two opposite open arms and two opposite closed arms (30 cm by 5 cm by 14 cm) arranged at right angles and with a common central platform (5 cm by 5 cm) that gave access to all arms. Lighting was maintained at 12 to 13 lux on the open arms and 3 to 4 lux in the closed arms. The experimental mouse was gently placed in the center of the maze looking toward a closed arm and allowed to move undisturbed for 5 min. After each trial, the arms were cleaned with 7% ethanol and dried. Video tracking of the animal's location was performed by a camera fixed above the arena. EthoVision tracking system was used to calculate the percentage of time spent in the open arms, which was taken as an indicator of anxiety.

Open field and novel object tests

The experimental mouse was placed in the corner of a rectangular arena (50 cm by 50 cm) and left to freely explore for 10 min (open field test phase). Afterward, a new object was placed in the center of the arena for 5 min (novel object test phase). Lighting was maintained at 8 to 10 lux on the center of the arena. After each trial, the arena was cleaned with 7% ethanol and dried. Video tracking of the animal's location was performed by a camera fixed above the arena. The percentage of time spent in the center of the open field was taken as an indicator of anxiety (open field test phase) or reactivity upon novelty (novel object test phase).

Saccharin preference test

To evaluate anhedonia, animals were placed individually in the TSE PhenoMaster system and habituated for 24 hours to a two-bottle choice condition before test. The automatic monitoring of liquid intake system was calibrated, and one bottle was filled with drinking water and the other with a solution of 0.05% saccharin (Sigma-Aldrich, #S1002). The system automatically calculated the liquid intake from each bottle for the next 48 hours. Saccharin preference was calculated as the percentage of volume of saccharin solution intake over the total volume of liquid intake (saccharin + water) over the 48 hours of testing.

Resident-intruder test

This test is designed to investigate aggression-related behavior toward an intruder. Experimental mice were cohabited with a female partner for 10 days before the day of the test, to encourage

territoriality. The female was removed 30 min before the onset of the test (conducted during the dark cycle) and placed back afterward. Mice were confronted with an intruder BALB/c in their home cages for 10 min. After an interval of 2 min, the intruders were reintroduced to the confrontation cages. Total offensive behaviors were manually scored afterward by an experienced researcher blinded to the experimental group.

Locomotor activity

Mice were placed individually in the TSE PhenoMaster system (TSE Systems), a caging system that contains infrared sensor frames configured to measure locomotor activity in the *x*, *y*, and *z* planes. The software records the number of beam interruptions caused by the animal's movement. Animals were habituated 24 hours in the cages before recording the locomotor activity for the next 48 hours.

Social interaction test

The social interaction test was used to assess social behavior. This is a two-step test, conducted under red light conditions. In the first 2.5-min session, the experimental mouse was allowed to freely explore and habituate to an open field arena (40 cm length by 40 cm width by 40 cm height). Along one side of the arena, there was a circular (7-cm-diameter) wire cage that remained empty during the first trial. The experimental mouse was then removed from the open field arena, and a novel unfamiliar CD1 male mouse was placed into the wire cage. In the second 2.5-min trial, the experimental mouse was reintroduced into the arena now containing a social target (unfamiliar CD1 mouse) within the wire cage. The percentage of time spent sniffing the unfamiliar CD1 mouse inside the wire cage was video-recorded and manually scored (Clicker, EPFL) by an experienced researcher blinded to the experimental group.

Determination of the estrous cycle phases

A noninvasive vaginal cytology was used to determine the phase of the estrous cycle in females after behavioral testing. Briefly, 10 µl of 0.9% NaCl (w/v) was softly released on the aperture of the vagina with a sterile pipette tip. Liquid was drawn back into the tip and slowly loaded again in the vagina for three consecutive times to collect enough cells. Next, the cell suspension was spread over a glass slide (Huberlab, #10.0230.01), air-dried and stained 5 min with 0.1% cresyl violet acetate (w/v) (Sigma-Aldrich, #C5042), and washed for 1 min in distilled water. Vaginal smears were examined immediately under a bright-field microscope (magnification, ×200). Estimation of the phase of the estrous cycle (proestrus/estrus or metestrus/diestrus) was based on the proportion of leucocytes, cornified epithelial cells, and nucleated epithelial cells (*77*).

Food intake

Food intake per mouse and day was measured as the difference in weight between the food added into the cage and that remaining at the end of 7 days, divided by 4 (number of mice per cage) and 7 (number of days).

Body composition

Whole-body composition was determined by nuclear magnetic resonance–based technology (EchoMRI, Echo Medical Systems). Each mouse was placed briefly (approximately 1 min, no anesthesia required) in the EchoMRI machine where lean and fat mass were recorded. Whole-body fat and lean content are expressed as a percentage of total body weight. For experiments including a peripubertal stress protocol, body composition was measured at PN27 (to counterbalance groups before stress exposure), PN43, and week 8. To counterbalance the experimental groups, another EchoMRI session was done between weeks 9 and 12, 2 days before surgery or pharmacological treatment (i.e., intracerebral cannulation, SIRT1 overexpression/knockdown, NAMPT overexpression, or systemic NMN). Animals were subjected to a last session of EchoMRI 2 days before behavioral testing or indirect calorimetry. Animals with an intracerebral cannula were not subjected to EchoMRI because of the incompatibility with metallic elements.

X-ray microCT

Abdominal fat volume was determined by x-ray microCT (Quantum Fx Micro CT, PerkinElmer), a noninvasive, quantitative technique to determine the spatial distribution of specific fat compartments. Scan conditions were set as follows: voltage = 90 kV, current = 160 µA, live = 80 µA, field of view = 24 mm, scan mode = fine (2 min), and voxel size = 50 µm. Anesthesia was maintained by mask inhalation of isoflurane vaporized at concentrations of up to 3% in the induction phase and at 1.5% during acute imaging procedure. Three-dimensional images were reconstructed and quantified using the visualization and imaging software Analyze 12.0 (AnalyzeDirect Inc., KS, USA) by an experienced researcher blinded to the experimental group. The abdominal muscular wall was used to separate visceral adipose tissue from subcutaneous adipose tissue. Fat depot volumes were normalized to the body weight of the mice (*78*).

Indirect calorimetry

The Comprehensive Lab Animal Monitoring System (CLAMS, Columbus Instruments) is a live-in cage system used for automated, noninvasive calorimetry assessment that provides measures of volume of O_2 (VO_2) consumed and volume of CO_2 (VCO_2) produced by the animal, energy expenditure (heat), and RER. RER is the ratio between VCO_2 and VO_2 (VCO_2/VO_2) and is a surrogate of substrate utilization. A value of 0.7 indicates a nearly complete dependence on fatty acid metabolism, while a value of 1.0 indicates primary dependence on carbohydrate metabolism. Mice were habituated to the cages for 24 hours, and the VO_2 and VCO_2 were recorded for the next 24 consecutive hours.

Morphologic analysis of adipocytes

eWAT was fixed in 4% formalin overnight and dehydrated in 70% ethanol. Within 48 hours following fixation, samples were embedded in paraffin, sectioned at 5 µm, and stained with hematoxylin and eosin. Sections were visualized on an Olympus Slide Scanner VS120-L100 (Olympus). Adipocytes were manually drawn and the area was quantified with ImageJ by an experienced researcher blinded to the experimental group. The adipocyte area of each mouse was measured at 8 to 10 random areas (176 µm by 176 µm) and averaged to generate the mean adipocyte area.

Intraperitoneal glucose tolerance test

The intraperitoneal glucose tolerance test measures the clearance of an intraperitoneally injected glucose load from the body. After an overnight fast, blood glucose concentration was determined with a glucometer (Accu-Check Aviva, Roche). Next, mice were injected intraperitoneally with a solution of glucose at a dose of 2 g/kg of body weight. After the injection, blood glucose was determined at different time points during the next 3 hours.

Insulin tolerance test

The insulin tolerance test is a standard test to determine the insulin resistance and the whole-body sensitivity of insulin receptors. After 6 hours of fast, blood glucose concentration was determined with a glucometer (Accu-Check Aviva, Roche). Next, mice were injected intraperitoneally with a solution of insulin (Umulin Rapid, Lilly, #HI0219) at a dose of 0.3 International unit (IU)/kg of body weight. After the injection, blood glucose was determined at different time points during the next 2 hours.

Genotyping

All *Sirt1*^{loxP} mice were genotyped twice, i.e., before weaning (from ear punches) and after sacrifice (from tail biopsies), by polymerase chain reaction (PCR) and the use of the following primers: 5-′GTTACCTATTGAACGCCCTAC-3 (forward) and GCCAACAAAGTTTAGATGTATCTAAGG (reverse).

Biochemical analysis of plasma

Enzyme-linked immunosorbent assay kits were used to measure plasma levels of eNAMPT (BioAim Scientific, #BA-2020003), adiponectin (Crystal Chem Inc., #80569), leptin (Enzo Life Sciences Inc., #ADI-900-019A), FGF-21 (R&D Systems, #MF2100), and GDF-15 (R&D Systems, #MGD150).

SIRT1 activity, SIRT1 gene expression, SIRT1 protein levels, and SIRT1 pathway activity

SIRT1 activity was measured with a fluorometric kit (see details in the "NAD^+ levels and SIRT1 activity assays" section) to validate the capacity of EX-527 to inhibit SIRT1 in the intracerebral cannulation experiments (see details in the "Intracerebral cannulation surgery" section). SIRT1 expression levels were measured either by real-time quantitative PCR (qPCR) using brain punches (see details in the "Brain punching" and "RNA extraction and quantitative real-time PCR" sections) or by in situ sequencing in brain slices (see details in the "In situ sequencing" section). SIRT1 protein levels were measured by immunofluorescence to validate the efficiency of the AAVs injected in the NAc to down-regulate or up-regulate SIRT1 protein levels (see details in the "SIRT1 immunofluorescence" section). Activation of the SIRT1 pathway was analyzed by measuring the expression levels of SIRT1 target genes (see details in the "Brain punching" and "RNA extraction and quantitative real-time PCR" sections) or by in situ sequencing in brain slices (see details in the "In situ sequencing" section).

Brain punching

Mice were decapitated, and brain was extracted and snap-frozen in isopentane at −45°C and stored at −80°C until further processing. The brains were sectioned on a freezing (−20°C) cryostat (Leica) and 150-μm-thick slices were mounted onto SuperFrost Plus Microscope Slides (Thermo Fisher Scientific). Different brain areas were dissected using 0.5- to 1.5-mm tissue punches (Harris UniCore). Coordinates were based on the atlas of Paxinos and Franklin (*79*) and were taken from bregma (in millimeters). NAc (1.5-mm punch): Anterior-Posterior (A.P.), 0.74 to 1.94; Medial-Lateral (M.L.), ± 0.25 to 1.75; Dorsal-Ventral (D.V.), −3.8 to −5.3; Arc (0.5-mm punch): A.P., −1.46 to −2.06; M.L., −0.25 to 0.25; D.V., −5.5 to −5.75 and A.P., −2.06 to −2.54; M.L., −0.5 to 0.5; D.V., −5.5 to −5.75; ventromedial hypothalamus (VMH) (0.5-mm punch): A.P., −1.34 to −1.94; M.L., ±0.25 to 0.75; D.V., −5.25 to −5.75 and A.P., -1.94 to −2.06; M.L., ±0.25 to 0.75; D.V., −5.5 to −6.0; BLA (0.5-mm punch): A.P., −0.58 to −1.94; M.L., ±2.5 to 3.0; D.V., −4.3 to −4.8; and ventral tegmental area (VTA) (0.5-mm punch): A.P., −2.92 to −3.64; M.L., ±0.25 to 0.75; D.V., −4.0 to −4.5. Tissue was collected in ribonuclease-free tubes and maintained in a −80°C freezer until further processing.

RNA extraction and quantitative real-time PCR

RNA from NAc punches was extracted using an Ambion RNaqueous-micro kit (Thermo Fisher Scientific, #AM1931) according to the manufacturer's recommendations. RNA from eWAT was extracted using the RNeasy Lipid Tissue Mini Kit (QIAGEN, #74804). RNA amount was quantified using a NanoDrop apparatus (Thermo Fisher Scientific). Complementary DNA was synthesized from total RNA (200 ng) using the qScript cDNA SuperMix (Quantabio, #95048) according to the supplier's recommendations. For real-time quantitative PCR, reactions were performed in triplicate using the Power SYBR Green PCR Master Mix (Thermo Fisher Scientific, #4367659) in an ABI Prism 7900 Sequence Detection system (Applied Biosystems, Life Technologies). Two genes were used as internal controls: TATA box–binding protein (*Tbp*) and eukaryotic elongation factor-1 (*Eef1*) for the NAc and *Tbp* and β-2 microglobulin (*B2m*) for the eWAT. Primers for the genes of interest were designed using National Center for Biotechnology Information primer design tool [Tbp (NM_013684.3): forward, CTGGAATTGTACCGCAGCTT; reverse, CAGTTGTCCGTGGCTCTCTT; Eef1a1 (NM_010106.2): forward, TCCACTTGGTCGCTTTGCT; reverse, CTTCTTGTCCACAGCTTTGATGA; B2m (NM_009735.3): forward, GGTCTTTCTGGTGCTTGTCTCA; reverse, GTTCGGCTTCCCATTCTCC; Sirt1 (NM_019812.3): forward, AAAAGATAATAGTTCTGACTGGAGCT; reverse, GGCGAGCATAGATACCGTCT; Tfam (NM_009360.4): forward, CCCCTCGTCTATCAGTCTTGTC; reverse, TTCTGGTAGCTCCCTCCACA; Nd1 (ENSMUST00000082392.1): forward, GGATGAGCCTCAAACTCCAA; reverse, GGTCAGGCTGGCAGAAGTAA; Nd6 (ENSMUST00000082419.1): forward, GGGGGATGTTGGTTGTGTTT; reverse, ACCAATCTCCCAAACCATCA; Atp6 (ENSMUSG00000064357.1): forward, CCTTCCACAAGGAACTCCAA; reverse, GGTAGCTGTTGGTGGGCTAA; Cat (NM_009804): forward, TTCGTCCCGAGTCTCTCCAT; reverse, ATGCCCTGGTCGGTCTTGTA; Prx3 (NM_007452): forward, CCCGGAGTATTTCTGCCTCA; reverse, GTGGAAAGAGGAACTGGTGCT; Nampt (NM_021524.2): forward, AAGGACCCAGTTGCTGATCC; reverse, ACCGTATGGAGAAGATCATGGC; Parp1 (NM_007415.2): forward, GGGCACAGTTATCGGCAGTA; reverse, CTTCGTCCTGGCCATAGTCAA; Nmnat1 (NM_133435.1): forward, AAACCAACAGGTGTGCCCAA; reverse, ATTTCTGAGCGTCACTGCCA; Nmnat2 (NM_175460.3): forward, ACTCCTACGGAAAACAGGGC; reverse, GGTCACCCTCTTCATCAGGTC]. Gene expression was analyzed using the comparative cycle threshold method.

Western blot

eWAT and liver were removed from euthanized mice and flash-frozen in liquid nitrogen. eWAT and liver tissue samples were lysed by mechanical homogenization for 1 min with radioimmunoprecipitation assay buffer [150 mM NaCl, 1% NP-40, 0.5% sodium deoxycholate, 0.1% SDS, and 50 mM tris (pH 8.0)] containing 1× protease (cOmplete Mini, EDTA-free Protease Inhibitor Cocktail; Roche, #11836170001) and 1× phosphatase inhibitors (PhosSTOP; Roche, #4906837001) in a pellet pestle (Fisherbrand Pellet Pestle Cordless Motor Adapter, Thermo Fisher Scientific, #12-141-362). Homogenates were sonicated

for 1 min and then centrifuged for 30 min at 16,000*g* at 4°C. The supernatant was collected for subsequent analysis. For the eWAT, the supernatant was collected with a syringe to avoid the upper layer of fat and centrifuged again for 30 min at 16,000*g* at 4°C. Protein concentration was analyzed with the DC Protein Assay (Bio-Rad Laboratories, #5000111) using bovine serum albumin (BSA) as the standard (Merck, #P5369), and samples were boiled for 5 min in loading buffer (New England Biolabs Inc., #B7703S). Protein homogenates (35 μg) were separated by SDS–polyacrylamide gel electrophoresis (Mini-PROTEAN Electrophoresis system, Bio-Rad) for 90 min at 120 mA, followed either by staining with Coomassie Brilliant Blue G-250 (EZ Blue Gel staining; Sigma-Aldrich, #G1041) or by transfer for 120 min at 200 mA onto 0.45-μm–pore size nitrocellulose membranes (Thermo Fisher Scientific, #88018). The membranes were incubated for 1 hour in Tris-buffered saline with 0.1% Tween® 20 Detergent (TBS-T) at room temperature [20 mM tris, 500 mM NaCl (pH 7.4), and 0.05% (v/v) Tween 20] plus 5% (w/v) nonfat dry milk (AppliChem GmbH, #A0830), washed with TBS-T, and incubated overnight at 4°C in a 1:5000 dilution of rabbit polyclonal anti-NAMPT antibody (Bethyl Laboratories Inc., #A300-372A) in TBS-T plus 5% (w/v) nonfat dry milk. The day after, membranes were washed with TBS-T and then incubated 1 hour at room temperature with a 1:5000 dilution of an horseradish peroxidase–conjugated goat anti-rabbit antibody (Invitrogen, #G21234) in TBS-T plus 5% (w/v) nonfat dry milk. Immunoreactive proteins were detected via enhanced chemiluminescence (SuperSignal West Dura Extended Duration Substrate, Thermo Fisher Scientific, #34076) and imaged using the Molecular Imager ChemiDoc XRS (Bio-Rad Laboratories, #170-8070). Homogeneous loading was monitored using the gel stained with Coomassie Brilliant Blue G-250. Pixel intensity was quantified using ImageJ software.

Mitochondrial respiration

Mice were euthanized by rapid decapitation and the NAc was rapidly dissected out, weighed, and placed in a petri dish on ice with 2 ml of relaxing solution [2.8 mM Ca_2K_2EGTA, 7.2 mM K_2EGTA, 5.8 mM ATP, 6.6 mM $MgCl_2$, 20 mM taurine, 15 mM sodium phosphocreatine, 20 mM imidazole, 0.5 mM dithiothreitol (DTT), and 50 mM MES (pH 7.1)] until further processing. Tissue samples were then gently homogenized in ice-cold respirometry medium [MiR05: 0.5 mM EGTA, 3 mM $MgCl_2$, 60 mM potassium lactobionate, 20 mM taurine, 10 mM KH_2PO_4, 20 mM Hepes, 110 mM sucrose, and 0.1% (w/v) BSA (pH 7.1)] with an eppendorf pestle. Then, 2 mg of tissue was used to measure mitochondrial respiration rates at 37°C using high-resolution respirometry (Oroboros Oxygraph 2K, Oroboros Instruments), as previously described (*45*). A substrate-uncoupler-inhibitor titration protocol was used to sequentially explore the various components of mitochondrial respiratory capacity. A nonphosphorylating resting state (Leak) was obtained after adding a mixture of malate (2 mM), pyruvate (10 mM), and glutamate (20 mM). To measure the respiration due to OXPHOS, we added substrates for the activation of specific complexes. Thus, oxygen flux due to CI was quantified by the addition of ADP (5 mM), followed by the addition of succinate (10 mM) to subsequently stimulate complex II (CI & CII). We then uncoupled respiration to examine the maximal capacity of the electron transport system using the protonophore and carbonylcyanide 4 (trifluoromethoxy) phenylhydrazone (successive titrations of 0.2 μM until maximal respiration rates were reached). We then examined consumption in the uncoupled state due solely to the activity of complex II (CII) by inhibiting complex I with the addition of rotenone (0.1 μM). Last, electron transport through complex III was inhibited by adding antimycin (2 μM) to obtain the level of residual O_2 consumption (ROX) due to oxidative side reactions outside of mitochondrial respiration. The O_2 flux obtained in each step of the protocol was normalized by the wet weight of the tissue sample used for the analysis and corrected for ROX.

NAD^+ levels and SIRT1 activity assays

NAD^+ from brain punches was extracted and measured using the EnzyChrom NAD^+/NADH Assay Kit (BioAssay Systems, #E2ND-100) according to the manufacturer's instructions. NAD^+ levels were normalized to protein content determined by the Lowry method. SIRT1 enzymatic activity was measured using the Fluor de Lys SIRT1 fluorometric drug discovery assay kit (Enzo Life Sciences Inc., #BML-AK555-0001). Briefly, NAc punches were mechanically homogenized with a pellet pestle in lysis buffer [20 mM Hepes (pH 7.4), 2 mM EGTA (pH 8), 1 mM DTT, 10% glycerol, 1% Triton X-100, 1 mM phenylmethylsulfonyl fluoride, and 1× Mini cOmplete Protease Inhibitor Cocktail], rotated end-over-end for 1 hour at 4°C, and sonicated. Next, 25 μg of protein (diluted in a total volume of 35 μl of assay buffer) was incubated with substrate solution (15 μl) for 45 min at room temperature with shaking. Last, developing solution (50 μl) was added and incubated for 30 min at 37°C. Fluorescence was measured with a microplate reader (excitation, 360 nm; emission, 465 nm; SaFire 2, Tecan).

Systemic NMN treatment

Nine-week-old mice had ad libitum access to NMN (BioVision Inc., #2733; purity ≥ 98% by high-performance liquid chromatography) dissolved in drinking water. On the basis of previously measured water consumption data, we estimated that mice received NMN (approximately 100 mg/kg per day). NMN was administered in the drinking water for 2.5 weeks. Water bottles were changed twice weekly.

SIRT1 immunofluorescence

Tissue preparation

Mice were deeply anesthetized with an overdose of sodium pentobarbital (Nembutal; 40 mg/kg, i.p.) and transcardially perfused with 40 ml of Ringer solution + heparin, followed by 100 ml of 4% paraformaldehyde (PFA) in 0.1 M phosphate buffer (PB, pH 7.4). Brains were postfixed in 4% PFA-PB overnight at 4°C and equilibrated in a solution of 30% sucrose in phosphate-buffered saline (PBS) for 1 day at 4°C Thereafter, brains were snap-frozen in isopentane at −45°C and stored at −80°C until further processing. Brains were sliced in coronal sections (30 μm thick) with a sliding cryostat (CM3050, Leica) and collected in cryoprotectant. For immunostaining, sections were rinsed in PBS, incubated for 5 min with 1% SDS in PBS, rinsed in PBS, and incubated for 1 hour with blocking solution [1% BSA (Sigma-Aldrich), 0.1% Triton X-100 (Sigma-Aldrich), and 5% normal donkey serum (Jackson ImmunoResearch Laboratories) in PBS buffer]. Sections were subsequently incubated overnight at 4°C with primary antibody (SIRT1 Antibody, Cell Signaling Technology, 1:200, #2028) in blocking solution. After rinsing in PBS, sections were incubated for 2 hours at room temperature with secondary antibody (donkey anti-rabbit immunoglobulin G Alexa Fluor 568; Thermo Fisher Scientific, #A-10042) in blocking solution. After washing with PBS, sections were counterstained with 4′,6-diamidino-2-phenylindole (DAPI; Sigma-Aldrich, 1:10,000 in PBS), rinsed with PBS, mounted

onto SuperFrost Plus Microscope Slides (Thermo Fisher Scientific), and coverslipped with Fluoromount-G (SouthernBiotech).

Image acquisition and analysis

Two to three brain sections containing the NAc were captured from each mouse. A mosaic of 16 images was captured with a confocal microscope (Zeiss LSM-700) using a 20× objective. Immunofluorescence laser scanning microscopy (LSM) images were stitched together using the grid stitching plug-in for Fiji. The background intensity of each channel was measured at five different random areas and averaged to generate a mean background that was subtracted from each channel. Cells were delineated using a Huang threshold to label only those stained with DAPI within 10 to 200 pixels. The number of cells that were colabeled with DAPI and SIRT1 was counted and converted to a percentage of the total number of SIRT1-stained cells for each section. To determine the efficiency of the viruses, the SIRT1 fluorescence intensity was measured in two manually drawn regions of interest (ROIs), one delimiting the whole NAc (ROI-1) and another delimiting the green fluorescent protein (GFP)–positive area within the NAc (ROI-2). The efficiency of the viruses (overexpression or down-regulation) was determined as the ratio of ROI-1 to ROI-2. Sections were then averaged to provide one value per animal and represented as a fold change with respect to the corresponding control virus. Quantification was performed on original, unenhanced images only and blind to experimental conditions. For visualization purposes, representative regions within specific sections were zoomed and enhanced in a linear manner for brightness and contrast using Adobe Photoshop.

Intracerebral cannulation surgery

Mice aged 9 to 10 weeks subjected to pharmacological experiments were implanted with bilateral guide cannulas aimed at the NAc. Before surgery, mice received an injection of analgesic (buprenorphine, temgesic at 0.1 mg/kg) and were anesthetized by isoflurane inhalation (induction 4% isoflurane and maintenance 2.5% isoflurane in O_2 at a flow of 4 liters/min) and placed in a stereotaxic apparatus (David Kopf Instruments). Small holes were drilled through the skull for bilateral placement of stainless steel 26-gauge guide cannula with pedestal (Plastics One, #C235GS-5-2.0) fitted with a removable dummy cannula. Coordinates were based on the atlas of Paxinos and Franklin (*79*) and were taken from bregma (in millimeters): A.P., +1.5; M.L., ±0,75; D.V., −3.50. Cannulas were fixed to the skull with one anchoring screw and dental acrylic (DuraLay Reliance, #2244). Mice were single-housed after surgery, treated with paracetamol (200 to 300 mg/kg, Dafalgan) via the drinking water for 7 days after the surgery, and allowed to recover for at least 10 days. For intracerebral infusions, the dummy was removed, and a 33-gauge injector (Plastics One, #C235IS-5) that extended 1 mm from the tip of the cannula was inserted aiming at the NAc [coordinates taken from bregma (in millimeters): A.P., +1.5; M.L., ±0.75; D.V., −4.50)]. Behavioral experiments were performed 1 hour after drug administration. Animals were randomly assigned to their respective treatment, and groups were counterbalanced for body weight. All drugs and vehicle were bilaterally infused in a total volume of 0.5 µl during 2.5 min of constant flow (0.2 µl/min). The injector remained in place for one additional minute after infusion to allow proper diffusion. NMN (Sigma-Aldrich, #N3501) was dissolved in saline with 0.5% dimethyl sulfoxide (DMSO) at a concentration of 25 mM. EX-527 (Sigma-Aldrich, #E7034) was dissolved in saline with 0.5% DMSO at a concentration of 0.5 mM. NMN and EX-527 were dissolved in saline with 0.5% DMSO at a concentration of 25 and 0.5 mM, respectively. Animals in the vehicle group were bilaterally infused with saline with 0.5% DMSO. After behavioral experiments, animals were euthanized by decapitation, and correct cannula placement was routinely verified with Cresyl violet histology. Images were captured using a bright-field slide scanner (Olympus VS120-L100). Mice that were not successfully targeted into the NAc were excluded from analysis.

Brain surgery and AAV-mediated gene transfer

AAV-mediated gene transfer was performed in mice aged 9 to 10 weeks. Groups were counterbalanced for body weight and body composition. Before surgery, mice received an injection of analgesic (buprenorphine, temgesic at 0.1 mg/kg) and were anesthetized by isoflurane inhalation (induction of 4% isoflurane and maintenance of 2.5% isoflurane in O_2 at a flow of 4 liters/min) and placed in a stereotaxic apparatus (David Kopf Instruments, Tujunga, CA, USA). AAV solution (1 µl; 1:2 dilution of stock AAV solution in saline) was infused at a rate of 0.1 µl/min using a Hamilton syringe (Hamilton Bonanduz AG) fitted with a 33-gauge needle aimed at the NAc (coordinates taken from bregma in millimeters: A.P., +1.6; M.L., ±1; D.V., −4.8). The needle was left in place for an additional 10 min before being slowly withdrawn. Mice receiving viral injections were treated with paracetamol (200 to 300 mg/kg, Dafalgan) for 7 days and allowed to recover for at least 3 weeks. For the SIRT1 overexpression experiments, we used the virus AAV2-Synapsin–enhanced GFP (eGFP)–2A-mouseSIRT1 (Vector Biolabs). For the SIRT1 knockout experiments, we used the virus AAV2-SYN-eGFP-T2A-iCre-WPRE (woodchuck posttranscriptional regulatory element) (Vector Biolabs). Both eGFP and SIRT1 (in the AAV2-SYN-eGFP-2A-mouseSIRT1 vector) and eGFP and iCre (codon-improved Cre) (in the AAV2-SYN-eGFP-T2A-iCre-WPRE) were driven by the same synapsin promoter with a 2A peptide linker in between for "self-cleavage" coexpression. WPRE enhancer was placed between the stop codon and the bGH polyA. As control AAV, we used the AAV2-SYN-eGFP-WPRE vector in both experiments. Viral injection site was verified in all mice by confirming GFP signal in the NAc coronal sections (30 µm thick) using a slide scanner (Olympus VS120-L100). Mice that were not successfully targeted into the NAc were excluded from analysis.

AS/Rec2-NAMPT vector and administration

The dual-cassette adipose-specific vector (AS/Rec2) contains an expression cassette consisting of the cytomegalovirus enhancer and chicken β-actin promoter, WPRE, and bovine growth hormone poly-A flanked by AAV2-inverted terminal repeats. A second cassette encoding a microRNA-WPRE driven by the albumin promoter that prevents transgene expression in the liver was cloned to the expression plasmid to generate the dual-cassette plasmid (fig. S6A). Vectors were constructed by Cao's laboratory as previously described (*80*). Mice at 9 to 12 weeks of age received a single intraperitoneal injection of the recombinant AAV AS/Rec2-Empty (same expression cassette with no transgene) or AS/Rec2 expressing NAMPT (AS/Rec2-NAMPT) at a dose of 2.0×10^{10} viral genomes diluted in viral dilution buffer to a volume of 100 µl. Groups were counterbalanced for body weight and body composition. Transduction of the adipose tissue with the AS/Rec2 virus was checked by the presence of the regulatory element WPRE by real-time qPCR using the following primers: TGGCGTGGTGTGCACTGT (forward) and GTTCCGCCGTGGCAATAG (reverse).

Electrophysiology

Acute coronal brain slices (220 μm thick) containing the NAc were prepared from control and stressed mice aged between 9 and 14 weeks. Animals were anesthetized with isoflurane and decapitated. The brain was quickly removed and cut using a vibrating tissue slicer (Campden Instruments) in oxygenated (95% O_2/5% CO_2) ice-cold modified artificial cerebrospinal fluid (ACSF), containing 105 mM sucrose, 65 mM NaCl, 25 mM $NaHCO_3$, 2.5 mM KCl, 1.25 mM NaH_2PO_4, 7 mM $MgCl_2$, 0.5 mM $CaCl_2$, 25 mM glucose, and 1.7 mM L(+)-ascorbic acid. Slices recovered for 1 hour at 35°C in standard ACSF containing 130 mM NaCl, 25 mM $NaHCO_3$, 2.5 mM KCl, 1.25 mM NaH_2PO_4, 1.2 mM $MgCl_2$, 2 mM $CaCl_2$, 18 mM glucose, and 1.7 mM L(+)-ascorbic acid, and complemented with 2 mM Na-pyruvate and 3 mM myo-inositol. In the recording chamber, slices were superfused with oxygenated standard ACSF at nearly physiological temperature (30° to 32°C). MSNs in the NAc shell were patched in the whole-cell configuration with borosilicate pipettes (2 to 3 megohms) filled with an intracellular solution containing 135 mM K-Gluconate, 10 mM KCl, 10 mM Hepes, 0.2 mM EGTA, 1.5 mM Mg-ATP, 0.2 mM Na-GTP, and 0.1% biocytin (290 to 300 mosmol, pH 7.2 to 7.3). To elicit neuronal firing, cells were held at −60 mV in current clamp configuration with direct current injections, and depolarization was provided by 2-s-long current steps or by 5-s-long current ramps of increasing magnitude. Electrophysiological data were acquired through a Digidata 1550A digitizer. The rheobase (minimal current required to elicit spiking) and the firing threshold were measured as the level of current and voltage, respectively, that induced the first action potential in the ramp protocol. Signals were amplified through a Multiclamp700B amplifier (Molecular Devices), sampled at 20 kHz and filtered at 10 kHz using Clampex10 (Molecular Devices). At the end of the recording, the patch pipette was gently retracted from the cell body to allow for membrane resealing. Slices were fixated in 4% PFA overnight and subsequently stored in a solution of 30% sucrose in PBS.

Neuronal dendritic arborization

Coronal brain slices used for electrophysiology recordings were washed (three times for 5 min at room temperature) in PBS and incubated (overnight at 4°C) with streptavidin–Alexa Fluor 488 (Thermo Fisher Scientific, S-11223, 1:500) in PBS–Triton X-100 0.05% to visualize the biocytin-filled MSNs. The next day, slices were washed (three times for 5 min at room temperature) in PBS and mounted in SuperFrost Plus Adhesion Microscope Slides (Thermo Fisher Scientific). Images of the biocytin-filled neurons were obtained with a confocal microscope (Zeiss LSM-700) using a 20× objective. Representative maximal intensity projections of *Z*-stack images were used to count the number of dendritic intersections at a fixed distance from the soma in concentric circles using the Sholl analysis tool from Fiji software.

In situ sequencing

In situ sequencing (ISS) technology enables the analysis of multiple genes with subcellular resolution, at their original location in morphologically preserved tissue sections. ISS was performed by CARTANA AB (Solna, Sweden). Briefly, fresh frozen brains were cryosectioned coronally into 10-μm-thick sections (AP, +1.0 to +1.3) and layered onto SuperFrost Plus Adhesion Microscope Slides and further stored at −80°C before experiments. A total of 12 mouse brain slices [control + AS/Rec2-Empty (n = 3), control + AS/Rec2-NAMPT (n = 2), Stress + AS/Rec2-Empty (n = 3), and Stress + AS/Rec2-NAMPT (n = 4)] were layered in four different glass slides (preparations). Slices were shipped on dry ice to CARTANA for tissue fixation, reverse transcription, barcoded probe hybridization and ligation onto target cDNA, rolling cycle amplification, barcode sequencing by six cycles of in situ sequencing chemistry, and fluorescence imaging by 40× objective and DAPI staining (*81*, *82*). A table of spatial coordinates of each read of the 33 genes analyzed together with the reference DAPI image per sample and the cell segmentation were provided by CARTANA. The panel of genes analyzed included cell-type markers (10 genes), *Sirt1*, and SIRT1 target genes (23 genes). Cell-type marker genes were selected based on single-cell RNA sequencing studies in mice NAc (*83*, *84*) and include *Drd1* and *Tac1* for MSN expressing dopamine D1-type receptors (D1-MSN), *Drd2* and *Penk* for MSN expressing dopamine 2-type receptors (D2-MSN), *Aqp4* and *Slc1a2* for astrocytes, *Plp1* and *Mbp* for oligodendrocytes, and *Itgam* and *Ctss* for microglia. SIRT1 target genes include genes involved in mitochondrial biogenesis and respiration (i.e., *Ppargc1a*, *Tfam*, *Ndufs4*, *Shda*, *Uqcrb*, *Cox6a2*, *Nd1*, *Nd6*, *Atp6*, *Aco2*, and *Cs*) (*85*, *86*), mitochondrial dynamics (i.e., *Mfn1*, *Mfn2*, and *Bnip3*) (*22*, *87*), oxidative stress response (i.e., *Cat* and *Gpx4*) (*85*, *88*), mtUPR (i.e., *Hspd1* and *Clpp*) (*89*), and neural signaling and activity [i.e., *Bdnf* and *Npy* (*22*), and *Hcrtr2* and *Kcnmb2* (*50*)]. The DAPI nucleus staining was used to segment individual cells and assign gene reads by spatial proximity. A read was assigned to the closest cell, except when such distance exceeds 300 pixels (=50 μm) from the DAPI centroid. A matrix of cells × gene reads corresponding to the NAc (whole), NAc shell, and NAc core were extracted using MATLAB (Image Processing Toolbox). To test whether a gene of interest was significantly different between two conditions, we used a generalized linear mixed-effects model. We used the number of reads, in each cell, of each gene as the dependent variable and the experimental and the group comparison as the fixed effect. A random intercept variable was used to account for the different preparations. Because the number of reads is count data, we modeled it with a Poisson distribution and a log link function. For each gene, three comparisons were performed: control versus stress mice receiving the AS/Rec2-Empty (effect of stress in animals injected with the empty virus); stressed mice injected either with AS/Rec2-Empty or AS/Rec2-NAMPT (effect of "NAMPT" in stressed animals); and AS/Rec2-Empty versus AS/Rec2-NAMPT in control nonstressed animals (effect of NAMPT in nonstressed animals). The MATLAB function fitglme was used to fit the count data of each gene using the restricted maximum pseudo-likelihood method. We used the coefficient estimate for the fixed effect to assess the enrichment or depletion of each gene due to each comparison. To increase the statistical power, we built seven composite scores that cluster genes belonging to the same biological pathway. The first composite, named "SIRT1 pathway," encompasses all the SIRT1 target genes analyzed. Two main gene composites were created afterward, named "mitochondrial function" (i.e., *Ppargc1a*, *Tfam*, *Ndufs4*, *Shda*, *Uqcrb*, *Cox6a2*, *Nd1*, *Nd6*, *Atp6*, *Aco2*, *Cs*, *Mfn1*, *Mfn2*, *Bnip3*, *Ca*t, *Gpx4*, *Hsp60*, and *Clpp*) and "neuronal activity" (i.e., *Bdnf*, *Npy*, *Hcrtr2*, and *Kcnmb2*). The composite mitochondrial function was subdivided into four subcomposites. The composite "mitochondrial biogenesis–OXPHOS (nDNA)" encompasses *Sirt1*, *Ppargc1a*, *Ndufs4*, *Shda*, *Uqcrb*, and *Cox6a2* and the composite "OXPHOS (mtDNA)" encompasses *Tfam*, *Nd1*, *Nd6*, and *Atp6*, which are transcriptional regulators of the mitochondrial

biogenesis and complex subunits of the OXPHOS system encoded by the nuclear DNA (nDNA) or the mitochondrial DNA (mtDNA), respectively. The composite "mitochondrial dynamics, TCA cycle, and antioxidants" includes *Mfn1*, *Mfn2*, *Bnip3*, *Aco2*, *Cs*, *Cat*, and *Gpx4* and the composite "mtUPR" includes *Hspd1* and *Clpp*. To compute the composite, gene reads were scaled to the interval between 0 and 1 and averaged to create composite scores. To have composite scores compatible with count data, these were lastly rescaled to count units by dividing by the lowest nonzero value and rounding to the nearest integer. Fixed-effect estimates of each group comparison on each gene/composite and their SEs are plotted in the figures. All *P* values were corrected for multiple comparisons using the false discovery rate (FDR) for 30 genes/composites × 3 conditions. Cell-specific analysis was performed for reads belonging to D1-MSN, D2-MSN, and MSN expressing both D1- and D2-type receptors (D1/D2-MSN), astrocytes, microglia, and oligodendrocytes. The same generalized linear mixed-effects model described above was used to analyze each cell type. For the cell-specific analysis, only two comparisons were performed: control versus stress mice receiving the AS/Rec2-Empty (effect of stress in animals injected with the empty virus) and stress + AS/Rec2-Empty versus AS/Rec2-NAMPT (effect of NAMPT in stressed animals). All *P* values were corrected for multiple comparisons using FDR for 30 genes/composites × 2 conditions × 6 cell types. Only significant *P* values ($P < 0.05$) are shown in the cell assignment plots.

Statistical analysis

Statistical analyses for the in situ sequencing are described in the "In situ sequencing" section. For the other analysis, detailed parameters from statistical tests are reported in the corresponding figure legend or in tables S1 to S7. Data are presented as means ± SEM, boxplot (interquartile range with whiskers showing the minimum to maximum range), or estimated marginal means ± SEM. No power analysis was performed to determine the sample size. The sample size in each study was based on previous experience in our lab. *N* represents the number of independent animals except for electrophysiological recordings and analysis of dendritic arborization where *N* represents the number of independent cells and food intake where *N* represents the number of independent cages. All statistical analyses were performed with Prism 8 (GraphPad Software Inc.) except for the analysis of covariance (ANCOVA) and linear mixed model that was performed with SPSS 22 (IBM). Shapiro-Wilk normality test was used to test normality. Unpaired two-tailed *t* (normally distributed data) test or Mann-Whitney rank sum test (non-normally distributed data) was used to compare two sets of data obtained from independent groups of animals. Welch correction was applied to normally distributed data when variances among groups were unequal. For more than two independent groups, we applied one-way analysis of variance (ANOVA) to analyze the effect of stress, as well as treatment and interaction when applicable. For two-factor comparison, two-way ANOVA was used to analyze the effect of stress, as well as treatment and interaction when applicable. ANCOVA was used for analysis of gas exchange and energy expenditure in calorimetry studies (absolute lean mass as covariate) (*90*) and analysis of body composition after injection of AS/Rec2-NAMPT viruses (age as covariate). *P* values were corrected for multiple comparisons using the Holm-Sidak method. All $P < 0.05$ were considered to be significant. $^{*}P < 0.05$; $^{**}P \leq 0.01$; $^{***}P \leq 0.001$. For data exclusion, Grubbs' test for outliers was performed in GraphPad with an α level of 0.05.

SUPPLEMENTARY MATERIALS

Supplementary material for this article is available at https://science.org/doi/10.1126/sciadv.abj9109

View/request a protocol for this paper from *Bio-protocol*.

REFERENCES AND NOTES

1. L. P. Spear, The adolescent brain and age-related behavioral manifestations. *Neurosci. Biobehav. Rev.* **24**, 417–463 (2000).
2. B. Holtrup, C. D. Church, R. Berry, L. Colman, E. Jeffery, J. Bober, M. S. Rodeheffer, Puberty is an important developmental period for the establishment of adipose tissue mass and metabolic homeostasis. *Adipocyte* **6**, 224–233 (2017).
3. C. Sandi, J. Haller, Stress and the social brain: Behavioural effects and neurobiological mechanisms. *Nat. Rev. Neurosci.* **16**, 290–304 (2015).
4. C. Heim, E. B. Binder, Current research trends in early life stress and depression: Review of human studies on sensitive periods, gene-environment interactions, and epigenetics. *Exp. Neurol.* **233**, 102–111 (2012).
5. L. Li, R. A. Chassan, E. H. Bruer, B. A. Gower, R. C. Shelton, Childhood maltreatment increases the risk for visceral obesity. *Obesity (Silver Spring)* **23**, 1625–1632 (2015).
6. A. Danese, M. Tan, Childhood maltreatment and obesity: Systematic review and meta-analysis. *Mol. Psychiatry* **19**, 544–554 (2014).
7. K. J. Rotenberg, C. Bharathi, H. Davies, T. Finch, Obesity and the social withdrawal syndrome. *Eat. Behav.* **26**, 167–170 (2017).
8. C. Varela, A. Andres, C. Saldana, The behavioral pathway model to overweight and obesity: Coping strategies, eating behaviors and body mass index. *Eat. Weight Disord.* **25**, 1277–1283 (2020).
9. J. Spahlholz, N. Baer, H. H. Konig, S. G. Riedel-Heller, C. Luck-Sikorski, Obesity and discrimination—A systematic review and meta-analysis of observational studies. *Obes. Rev.* **17**, 43–55 (2016).
10. J. H. Stern, J. M. Rutkowski, P. E. Scherer, Adiponectin, leptin, and fatty acids in the maintenance of metabolic homeostasis through adipose tissue crosstalk. *Cell Metab.* **23**, 770–784 (2016).
11. A. Garten, S. Schuster, M. Penke, T. Gorski, T. de Giorgis, W. Kiess, Physiological and pathophysiological roles of NAMPT and NAD metabolism. *Nat. Rev. Endocrinol.* **11**, 535–546 (2015).
12. E. Verdin, NAD^+ in aging, metabolism, and neurodegeneration. *Science* **350**, 1208–1213 (2015).
13. M. J. Yoon, M. Yoshida, S. Johnson, A. Takikawa, I. Usui, K. Tobe, T. Nakagawa, J. Yoshino, S. Imai, SIRT1-mediated eNAMPT secretion from adipose tissue regulates hypothalamic NAD+ and function in mice. *Cell Metab.* **21**, 706–717 (2015).
14. M. Yoshida, A. Satoh, J. B. Lin, K. F. Mills, Y. Sasaki, N. Rensing, M. Wong, R. S. Apte, S. I. Imai, Extracellular vesicle-contained eNAMPT delays aging and extends lifespan in mice. *Cell Metab.* **30**, 329–342.e5 (2019).
15. A. Z. Herskovits, L. Guarente, SIRT1 in neurodevelopment and brain senescence. *Neuron* **81**, 471–483 (2014).
16. J. Yoshino, J. A. Baur, S. I. Imai, NAD^+ intermediates: The biology and therapeutic potential of NMN and NR. *Cell Metab.* **27**, 513–528 (2018).
17. G. Dolen, A. Darvishzadeh, K. W. Huang, R. C. Malenka, Social reward requires coordinated activity of nucleus accumbens oxytocin and serotonin. *Nature* **501**, 179–184 (2013).
18. P. J. Lucassen, J. Pruessner, N. Sousa, O. F. X. Almeida, A. M. Van Dam, G. Rajkowska, D. F. Swaab, B. Czéh, Neuropathology of stress. *Acta Neuropathol.* **127**, 109–135 (2014).
19. J. N. Feige, J. Auwerx, Transcriptional targets of sirtuins in the coordination of mammalian physiology. *Curr. Opin. Cell Biol.* **20**, 303–309 (2008).
20. E. Katsyuba, M. Romani, D. Hofer, J. Auwerx, NAD^+ homeostasis in health and disease. *Nat. Metab.* **2**, 9–31 (2020).
21. H. D. Kim, J. Hesterman, T. Call, S. Magazu, E. Keeley, K. Armenta, H. Kronman, R. L. Neve, E. J. Nestler, D. Ferguson, SIRT1 mediates depression-like behaviors in the nucleus accumbens. *J. Neurosci.* **36**, 8441–8452 (2016).
22. D. Ferguson, N. Shao, E. Heller, J. Feng, R. Neve, H. D. Kim, T. Call, S. Magazu, L. Shen, E. J. Nestler, SIRT1-FOXO3a regulate cocaine actions in the nucleus accumbens. *J. Neurosci.* **35**, 3100–3111 (2015).
23. L. Nielsen, M. Mather, Emerging perspectives in social neuroscience and neuroeconomics of aging. *Soc. Cogn. Affect. Neurosci.* **6**, 149–164 (2011).
24. D. Kaufman, M. A. Banerji, I. Shorman, E. L. Smith, J. D. Coplan, L. A. Rosenblum, J. G. Kral, Early-life stress and the development of obesity and insulin resistance in juvenile bonnet macaques. *Diabetes* **56**, 1382–1386 (2007).
25. L. Germine, E. C. Dunn, K. A. McLaughlin, J. W. Smoller, Childhood adversity is associated with adult theory of mind and social affiliation, but not face processing. *PLOS ONE* **10**, e0129612 (2015).
26. K. L. Spalding, E. Arner, P. O. Westermark, S. Bernard, B. A. Buchholz, O. Bergmann, L. Blomqvist, J. Hoffstedt, E. Naslund, T. Britton, H. Concha, M. Hassan, M. Ryden, J. Frisen, P. Arner, Dynamics of fat cell turnover in humans. *Nature* **453**, 783–787 (2008).

27. L. S. Adair, Child and adolescent obesity: Epidemiology and developmental perspectives. *Physiol. Behav.* **94**, 8–16 (2008).
28. K. Y. Yam, E. F. G. Naninck, M. R. Abbink, S. E. la Fleur, L. Schipper, J. C. van den Beukel, A. Grefhorst, A. Oosting, E. M. van der Beek, P. J. Lucassen, A. Korosi, Exposure to chronic early-life stress lastingly alters the adipose tissue, the leptin system and changes the vulnerability to western-style diet later in life in mice. *Psychoneuroendocrinology* **77**, 186–195 (2017).
29. N. P. Daskalakis, R. C. Bagot, K. J. Parker, C. H. Vinkers, E. R. de Kloet, The three-hit concept of vulnerability and resilience: Toward understanding adaptation to early-life adversity outcome. *Psychoneuroendocrinology* **38**, 1858–1873 (2013).
30. J. Liu, M. Guo, D. Zhang, S. Y. Cheng, M. Liu, J. Ding, P. E. Scherer, F. Liu, X. Y. Lu, Adiponectin is critical in determining susceptibility to depressive behaviors and has antidepressant-like activity. *Proc. Natl. Acad. Sci. U.S.A.* **109**, 12248–12253 (2012).
31. J. Yoshino, K. F. Mills, M. J. Yoon, S. Imai, Nicotinamide mononucleotide, a key NAD^+ intermediate, treats the pathophysiology of diet- and age-induced diabetes in mice. *Cell Metab.* **14**, 528–536 (2011).
32. A. Chalkiadaki, L. Guarente, High-fat diet triggers inflammation-induced cleavage of SIRT1 in adipose tissue to promote metabolic dysfunction. *Cell Metab.* **16**, 180–188 (2012).
33. S. Jukarainen, S. Heinonen, J. T. Ramo, R. Rinnankoski-Tuikka, E. Rappou, M. Tummers, M. Muniandy, A. Hakkarainen, J. Lundbom, N. Lundbom, J. Kaprio, A. Rissanen, E. Pirinen, K. H. Pietilainen, Obesity is associated with low NAD^+/SIRT pathway expression in adipose tissue of BMI-discordant monozygotic twins. *J. Clin. Endocrinol. Metab.* **101**, 275–283 (2016).
34. C. Pagano, C. Pilon, M. Olivieri, P. Mason, R. Fabris, R. Serra, G. Milan, M. Rossato, G. Federspil, R. Vettor, Reduced plasma visfatin/pre-B cell colony-enhancing factor in obesity is not related to insulin resistance in humans. *J. Clin. Endocrinol. Metab.* **91**, 3165–3170 (2006).
35. Y. H. Chang, D. M. Chang, K. C. Lin, S. J. Shin, Y. J. Lee, Visfatin in overweight/obesity, type 2 diabetes mellitus, insulin resistance, metabolic syndrome and cardiovascular diseases: A meta-analysis and systemic review. *Diabetes Metab. Res. Rev.* **27**, 515–527 (2011).
36. J. Berndt, N. Kloting, S. Kralisch, P. Kovacs, M. Fasshauer, M. R. Schon, M. Stumvoll, M. Bluher, Plasma visfatin concentrations and fat depot-specific mRNA expression in humans. *Diabetes* **54**, 2911–2916 (2005).
37. E. Garcia-Fuentes, J. M. Garcia-Almeida, J. Garcia-Arnes, S. Garcia-Serrano, J. Rivas-Marin, J. L. Gallego-Perales, G. Rojo-Martinez, L. Garrido-Sanchez, F. J. Bermudez-Silva, F. Rodriguez de Fonseca, F. Soriguer, Plasma visfatin concentrations in severely obese subjects are increased after intestinal bypass. *Obesity* **15**, 2391–2395 (2007).
38. A. Esteghamati, A. Alamdari, A. Zandieh, S. Elahi, O. Khalilzadeh, M. Nakhjavani, A. Meysamie, Serum visfatin is associated with type 2 diabetes mellitus independent of insulin resistance and obesity. *Diabetes Res. Clin. Pract.* **91**, 154–158 (2011).
39. D. Lin, M. P. Boyle, P. Dollar, H. Lee, E. S. Lein, P. Perona, D. J. Anderson, Functional identification of an aggression locus in the mouse hypothalamus. *Nature* **470**, 221–226 (2011).
40. C. J. Pena, M. Smith, A. Ramakrishnan, H. M. Cates, R. C. Bagot, H. G. Kronman, B. Patel, A. B. Chang, I. Purushothaman, J. Dudley, H. Morishita, L. Shen, E. J. Nestler, Early life stress alters transcriptomic patterning across reward circuitry in male and female mice. *Nat. Commun.* **10**, 5098 (2019).
41. C. Menard, M. L. Pfau, G. E. Hodes, V. Kana, V. X. Wang, S. Bouchard, A. Takahashi, M. E. Flanigan, H. Aleyasin, K. B. LeClair, W. G. Janssen, B. Labonte, E. M. Parise, Z. S. Lorsch, S. A. Golden, M. Heshmati, C. Tamminga, G. Turecki, M. Campbell, Z. A. Fayad, C. Y. Tang, M. Merad, S. J. Russo, Social stress induces neurovascular pathology promoting depression. *Nat. Neurosci.* **20**, 1752–1760 (2017).
42. S. Nemoto, M. M. Fergusson, T. Finkel, Nutrient availability regulates SIRT1 through a forkhead-dependent pathway. *Science* **306**, 2105–2108 (2004).
43. R. Chen, E. M. Dioum, R. T. Hogg, R. D. Gerard, J. A. Garcia, Hypoxia increases sirtuin 1 expression in a hypoxia-inducible factor-dependent manner. *J. Biol. Chem.* **286**, 13869–13878 (2011).
44. E. Gebara, O. Zanoletti, S. Ghosal, J. Grosse, B. L. Schneider, G. Knott, S. Astori, C. Sandi, Mitofusin-2 in the nucleus accumbens regulates anxiety and depression-like behaviors through mitochondrial and neuronal actions. *Biol. Psychiatry* **89**, 1033–1044 (2021).
45. F. Hollis, M. A. van der Kooij, O. Zanoletti, L. Lozano, C. Canto, C. Sandi, Mitochondrial function in the brain links anxiety with social subordination. *Proc. Natl. Acad. Sci. U.S.A.* **112**, 15486–15491 (2015).
46. M. A. van der Kooij, F. Hollis, L. Lozano, I. Zalachoras, S. Abad, O. Zanoletti, J. Grosse, I. Guillot de Suduiraut, C. Canto, C. Sandi, Diazepam actions in the VTA enhance social dominance and mitochondrial function in the nucleus accumbens by activation of dopamine D1 receptors. *Mol. Psychiatry* **23**, 569–578 (2018).
47. L. A. Gunaydin, L. Grosenick, J. C. Finkelstein, I. V. Kauvar, L. E. Fenno, A. Adhikari, S. Lammel, J. J. Mirzabekov, R. D. Airan, K. A. Zalocusky, K. M. Tye, P. Anikeeva, R. C. Malenka, K. Deisseroth, Natural neural projection dynamics underlying social behavior. *Cell* **157**, 1535–1551 (2014).
48. T. C. Francis, R. Chandra, A. Gaynor, P. Konkalmatt, S. R. Metzbower, B. Evans, M. Engeln, T. A. Blanpied, M. K. Lobo, Molecular basis of dendritic atrophy and activity in stress susceptibility. *Mol. Psychiatry* **22**, 1512–1519 (2017).
49. A. Trevisiol, A. S. Saab, U. Winkler, G. Marx, H. Imamura, W. Mobius, K. Kusch, K. A. Nave, J. Hirrlinger, Monitoring ATP dynamics in electrically active white matter tracts. *eLife* **6**, (2017).
50. A. Satoh, C. S. Brace, G. Ben-Josef, T. West, D. F. Wozniak, D. M. Holtzman, E. D. Herzog, S. Imai, SIRT1 promotes the central adaptive response to diet restriction through activation of the dorsomedial and lateral nuclei of the hypothalamus. *J. Neurosci.* **30**, 10220–10232 (2010).
51. J. J. Harris, R. Jolivet, D. Attwell, Synaptic energy use and supply. *Neuron* **75**, 762–777 (2012).
52. M. Picard, B. S. McEwen, E. S. Epel, C. Sandi, An energetic view of stress: Focus on mitochondria. *Front. Neuroendocrinol.* **49**, 72–85 (2018).
53. A. Cherix, T. Larrieu, J. Grosse, J. Rodrigues, B. McEwen, C. Nasca, R. Gruetter, C. Sandi, Metabolic signature in nucleus accumbens for anti-depressant-like effects of acetyl-L-carnitine. *eLife* **9**, e50631 (2020).
54. T. Larrieu, A. Cherix, A. Duque, J. Rodrigues, H. Lei, R. Gruetter, C. Sandi, Hierarchical status predicts behavioral vulnerability and nucleus accumbens metabolic profile following chronic social defeat stress. *Curr. Biol.* **27**, 2202–2210.e4 (2017).
55. A. Strasser, L. Xin, R. Gruetter, C. Sandi, Nucleus accumbens neurochemistry in human anxiety: A 7 T ^{1}H-MRS study. *Eur. Neuropsychopharmacol.* **29**, 365–375 (2019).
56. L. Lo Iacono, F. Visco-Comandini, A. Valzania, M. T. Viscomi, M. Coviello, A. Giampa, L. Roscini, E. Bisicchia, A. Siracusano, A. Troisi, S. Puglisi-Allegra, V. Carola, Adversity in childhood and depression: Linked through SIRT1. *Transl. Psychiatry* **5**, e629 (2015).
57. R. Chandra, C. A. Calarco, M. K. Lobo, Differential mitochondrial morphology in ventral striatal projection neuron subtypes. *J. Neurosci. Res.* **97**, 1579–1589 (2019).
58. J. E. de la Rubia, E. Drehmer, J. L. Platero, M. Benlloch, J. Caplliure-Llopis, C. Villaron-Casales, N. de Bernardo, J. AlarcOn, C. Fuente, S. Carrera, D. Sancho, P. Garcla-Pardo, R. Pascual, M. JuArez, M. Cuerda-Ballester, A. Forner, S. Sancho-Castillo, C. Barrios, E. Obrador, P. Marchio, R. Salvador, H. E. Holmes, R. W. Dellinger, L. Guarente, J. M. Estrela, Efficacy and tolerability of EH301 for amyotrophic lateral sclerosis: A randomized, double-blind, placebo-controlled human pilot study. *Amyotroph. Lateral Scler. Frontotemporal Degener.* **20**, 115–122 (2019).
59. J. Irie, E. Inagaki, M. Fujita, H. Nakaya, M. Mitsuishi, S. Yamaguchi, K. Yamashita, S. Shigaki, T. Ono, H. Yukioka, H. Okano, Y. I. Nabeshima, S. I. Imai, M. Yasui, K. Tsubota, H. Itoh, Effect of oral administration of nicotinamide mononucleotide on clinical parameters and nicotinamide metabolite levels in healthy Japanese men. *Endocr. J.* **67**, 153–160 (2020).
60. S. J. Gardell, M. Hopf, A. Khan, M. Dispagna, E. Hampton Sessions, R. Falter, N. Kapoor, J. Brooks, J. Culver, C. Petucci, C. T. Ma, S. E. Cohen, J. Tanaka, E. S. Burgos, J. S. Hirschi, S. R. Smith, E. Sergienko, A. B. Pinkerton, Boosting NAD^+ with a small molecule that activates NAMPT. *Nat. Commun.* **10**, 3241 (2019).
61. C. Canto, J. Auwerx, Interference between PARPs and SIRT1: A novel approach to healthy ageing? *Aging* **3**, 543–547 (2011).
62. R. W. Logan, P. K. Parekh, G. N. Kaplan, D. D. Becker-Krail, W. P. Williams 3rd, S. Yamaguchi, J. Yoshino, M. A. Shelton, X. Zhu, H. Zhang, S. Waplinger, E. Fitzgerald, J. Oliver-Smith, P. Sundarvelu, J. F. Enwright III, Y. H. Huang, C. A. McClung, NAD+ cellular redox and SIRT1 regulate the diurnal rhythms of tyrosine hydroxylase and conditioned cocaine reward. *Mol. Psychiatry* **24**, 1668–1684 (2019).
63. B. Balakrishnan, D. Sen, S. Hareendran, V. Roshini, S. David, A. Srivastava, G. R. Jayandharan, Activation of the cellular unfolded protein response by recombinant adeno-associated virus vectors. *PLOS ONE* **8**, e53845 (2013).
64. K. K. Ridout, M. Levandowski, S. J. Ridout, L. Gantz, K. Goonan, D. Palermo, L. H. Price, A. R. Tyrka, Early life adversity and telomere length: A meta-analysis. *Mol. Psychiatry* **23**, 858–871 (2018).
65. A. Kupferberg, L. Bicks, G. Hasler, Social functioning in major depressive disorder. *Neurosci. Biobehav. Rev.* **69**, 313–332 (2016).
66. M. S. Speed, O. H. Jefsen, A. D. Borglum, D. Speed, S. D. Ostergaard, Investigating the association between body fat and depression via Mendelian randomization. *Transl. Psychiatry* **9**, 184 (2019).
67. P. Willner, A. Towell, D. Sampson, S. Sophokleous, R. Muscat, Reduction of sucrose preference by chronic unpredictable mild stress, and its restoration by a tricyclic antidepressant. *Psychopharmacology* **93**, 358–364 (1987).
68. P. Willner, Reliability of the chronic mild stress model of depression: A user survey. *Neurobiol. Stress* **6**, 68–77 (2017).
69. J. P. Bras, I. Guillot de Suduiraut, O. Zanoletti, S. Monari, M. Meijer, J. Grosse, M. A. Barbosa, S. G. Santos, C. Sandi, M. I. Almeida, Stress-induced depressive-like behavior in male rats is associated with microglial activation and inflammation dysregulation in the hippocampus in adulthood. *Brain Behav. Immun.* **99**, 397–408 (2022).

70. A. J. Peckett, D. C. Wright, M. C. Riddell, The effects of glucocorticoids on adipose tissue lipid metabolism. *Metabolism* **60**, 1500–1510 (2011).
71. S. Ognjanovic, S. Bao, S. Y. Yamamoto, J. Garibay-Tupas, B. Samal, G. D. Bryant-Greenwood, Genomic organization of the gene coding for human pre-B-cell colony enhancing factor and expression in human fetal membranes. *J. Mol. Endocrinol.* **26**, 107–117 (2001).
72. C. Y. Yu, O. Mayba, J. V. Lee, J. Tran, C. Harris, T. P. Speed, J. C. Wang, Genome-wide analysis of glucocorticoid receptor binding regions in adipocytes reveal gene network involved in triglyceride homeostasis. *PLOS ONE* **5**, e15188 (2010).
73. J. K. Corrigan, D. Ramachandran, Y. He, C. J. Palmer, M. J. Jurczak, R. Chen, B. Li, R. H. Friedline, J. K. Kim, J. J. Ramsey, L. Lantier, O. P. McGuinness; Mouse Metabolic Phenotyping Center Energy Balance Working Group, A. S. Banks, A big-data approach to understanding metabolic rate and response to obesity in laboratory mice. *eLife* **9**, e53560 (2020).
74. B. J. Ellis, M. Del Giudice, Developmental adaptation to stress: An evolutionary perspective. *Annu. Rev. Psychol.* **70**, 111–139 (2019).
75. Z. R. Patterson, A. Abizaid, Stress induced obesity: Lessons from rodent models of stress. *Front. Neurosci.* **7**, 130 (2013).
76. G. Lo Sasso, D. Ryu, L. Mouchiroud, S. C. Fernando, C. L. Anderson, E. Katsyuba, A. Piersigilli, M. O. Hottiger, K. Schoonjans, J. Auwerx, Loss of Sirt1 function improves intestinal anti-bacterial defense and protects from colitis-induced colorectal cancer. *PLOS ONE* **9**, e102495 (2014).
77. A. F. Ajayi, R. E. Akhigbe, Staging of the estrous cycle and induction of estrus in experimental rodents: An update. *Fertil. Res. Pract.* **6**, 5 (2020).
78. S. Judex, Y. K. Luu, E. Ozcivici, B. Adler, S. Lublinsky, C. T. Rubin, Quantification of adiposity in small rodents using micro-CT. *Methods* **50**, 14–19 (2010).
79. G. Paxinos, K. B. J. Franklin, K. B. J. Franklin, *The Mouse Brain in Stereotaxic Coordinates* (Academic Press, ed. 2, 2001).
80. W. Huang, X. Liu, N. J. Queen, L. Cao, Targeting visceral fat by intraperitoneal delivery of novel AAV serotype vector restricting off-target transduction in liver. *Mol. Ther. Methods Clin. Dev.* **6**, 68–78 (2017).
81. R. Ke, M. Mignardi, A. Pacureanu, J. Svedlund, J. Botling, C. Wahlby, M. Nilsson, In situ sequencing for RNA analysis in preserved tissue and cells. *Nat. Methods* **10**, 857–860 (2013).
82. W. T. Chen, A. Lu, K. Craessaerts, B. Pavie, C. Sala Frigerio, N. Corthout, X. Qian, J. Lalakova, M. Kuhnemund, I. Voytyuk, L. Wolfs, R. Mancuso, E. Salta, S. Balusu, A. Snellinx, S. Munck, A. Jurek, J. Fernandez Navarro, T. C. Saido, I. Huitinga, J. Lundeberg, M. Fiers, B. De Strooper, Spatial transcriptomics and in situ sequencing to study Alzheimer's disease. *Cell* **182**, 976–991.e19 (2020).
83. D. Avey, S. Sankararaman, A. K. Y. Yim, R. Barve, J. Milbrandt, R. D. Mitra, Single-cell RNA-seq uncovers a robust transcriptional response to morphine by glia. *Cell Rep.* **24**, 3619–3629.e4 (2018).
84. O. Gokce, G. M. Stanley, B. Treutlein, N. F. Neff, J. G. Camp, R. C. Malenka, P. E. Rothwell, M. V. Fuccillo, T. C. Sudhof, S. R. Quake, Cellular taxonomy of the mouse striatum as revealed by single-cell RNA-seq. *Cell Rep.* **16**, 1126–1137 (2016).
85. A. Brunet, L. B. Sweeney, J. F. Sturgill, K. F. Chua, P. L. Greer, Y. Lin, H. Tran, S. E. Ross, R. Mostoslavsky, H. Y. Cohen, L. S. Hu, H. L. Cheng, M. P. Jedrychowski, S. P. Gygi, D. A. Sinclair, F. W. Alt, M. E. Greenberg, Stress-dependent regulation of FOXO transcription factors by the SIRT1 deacetylase. *Science* **303**, 2011–2015 (2004).
86. Z. Gerhart-Hines, J. T. Rodgers, O. Bare, C. Lerin, S. H. Kim, R. Mostoslavsky, F. W. Alt, Z. Wu, P. Puigserver, Metabolic control of muscle mitochondrial function and fatty acid oxidation through SIRT1/PGC-1alpha. *EMBO J.* **26**, 1913–1923 (2007).
87. Y. Lei, J. Wang, D. Wang, C. Li, B. Liu, X. Fang, J. You, M. Guo, X. Y. Lu, SIRT1 in forebrain excitatory neurons produces sexually dimorphic effects on depression-related behaviors and modulates neuronal excitability and synaptic transmission in the medial prefrontal cortex. *Mol. Psychiatry* **25**, 1094–1111 (2020).
88. C. K. Singh, G. Chhabra, M. A. Ndiaye, L. M. Garcia-Peterson, N. J. Mack, N. Ahmad, The role of sirtuins in antioxidant and redox signaling. *Antioxid. Redox Signal.* **28**, 643–661 (2018).
89. L. Mouchiroud, R. H. Houtkooper, N. Moullan, E. Katsyuba, D. Ryu, C. Canto, A. Mottis, Y. S. Jo, M. Viswanathan, K. Schoonjans, L. Guarente, J. Auwerx, The NAD^+/sirtuin pathway modulates longevity through activation of mitochondrial UPR and FOXO signaling. *Cell* **154**, 430–441 (2013).
90. M. H. Tschop, J. R. Speakman, J. R. Arch, J. Auwerx, J. C. Bruning, L. Chan, R. H. Eckel, R. V. Farese Jr., J. E. Galgani, C. Hambly, M. A. Herman, T. L. Horvath, B. B. Kahn, S. C. Kozma, E. Maratos-Flier, T. D. Muller, H. Munzberg, P. T. Pfluger, L. Plum, M. L. Reitman, K. Rahmouni, G. I. Shulman, G. Thomas, C. R. Kahn, E. Ravussin, A guide to analysis of mouse energy metabolism. *Nat. Methods* **9**, 57–63 (2011).

Acknowledgments

Funding: This work was supported by grants from the Swiss National Science Foundation (SNSF) (176206; NCCR Synapsy: 51NF40-158776 and -185897) and ERA-NET (Biostress; SNSF no. 31NE30_189061) and funded by the Biostime Institute for Nutrition and Care—Geneva Funding Programs (call 2020) to C.S. L.M. was supported by EPFL Fellows Marie Skłodowska-Curie actions (MSCA) (no. 6656679); I.Z. was supported by EMBO long-term fellowship [ALTF 1537-2015; MSCA (LTFCOFUND2013, GA-2013-609409)]; and S.G. was supported by Eurotech EU Horizon 2020 (no. 754462). J.A. acknowledges support from the EPFL, the European Research Council (ERC-AdG-787702), and the SNSF (SNSF 310030B_160318 and 31003A_179435). L.C. was supported by grants from NIH (AG041250, CA166590, and CA163640). This work was supported in part using the resources and services of the Center of Phenogenomics at the School of Life Sciences of EPFL. **Author contributions:** L.M. and C.S. conceived the project with input from J.A. L.M. performed most experiments, analyzed the data, and interpreted results with support from I.Z., S.G., I.G.d.S., J.G., and O.Z. W.H. and L.C. generated rAAV. S.A. performed and analyzed electrophysiological recordings. J.R. analyzed in situ sequencing data. L.M. and C.S. wrote the manuscript. All authors discussed the results and edited and approved the manuscript. **Competing interests:** J.A. is a SAB member of MetroBiotech and Mitobridge-Astellas. All other authors declare that they have no competing interests. **Data and materials availability:** All data needed to evaluate the conclusions in the paper are present in the paper and/or the Supplementary Materials. Newly generated items include recombinant AAV (AS/Rec2) to overexpress NAMPT and can be provided by L.C. with pending scientific review and a completed material transfer agreement (MTA).

Submitted 9 June 2021
Accepted 5 January 2022
Published 2 March 2022
10.1126/sciadv.abj9109

ScienceAdvances

eNAMPT actions through nucleus accumbens NAD/SIRT1 link increased adiposity with sociability deficits programmed by peripuberty stress

Laia MoratóSimone AstoriIoannis ZalachorasJoao RodriguesSriparna GhosalWei HuangIsabelle Guillot de SuduirautJocelyn GrosseOlivia ZanolettiLei CaoJohan AuwerxCarmen Sandi

Sci. Adv., 8 (9), eabj9109. • DOI: 10.1126/sciadv.abj9109

Science Advances (ISSN) is published by the American Association for the Advancement of Science. 1200 New York Avenue NW, Washington, DC 20005. The title *Science Advances* is a registered trademark of AAAS.